Engineering Structures 322 (2025) 118885

Contents lists available at ScienceDirect

Engineering Structures

journal homepage: www.elsevier.com/locate/engstruct

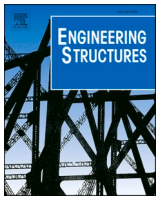

Stochastic analysis of combined primary-secondary structures subjected to imprecise seismic excitation

Alba Sofi [a,*], Federica Genovese [b]

[a] Department of Architecture and Territory and Inter-University Centre of Theoretical and Experimental Dynamics, University "Mediterranea" of Reggio Calabria, Via dell'Università 25, 89124 Reggio Calabria, Italy
[b] Department of Architecture and Territory, University "Mediterranea" of Reggio Calabria, Via dell'Università 25, 89124 Reggio Calabria, Italy

ARTICLE INFO

Keywords:
Combined primary-secondary structures
Interval analysis
Random excitation
Imprecise *Power Spectral Density* function
Interval *reliability function*

ABSTRACT

The imprecise stochastic process model is able to incorporate both random and epistemic uncertainties, leading to a more accurate description of environmental excitations, such as earthquakes or wind loads, when limited data are available. Epistemic uncertainties in the loading model may significantly affect the performance of structural systems.

The present paper addresses the stochastic analysis of combined primary-secondary structures subjected to imprecise seismic excitation modeled as a zero-mean stationary Gaussian random process, characterized by an interval-valued *Power Spectral Density* (*PSD*) function. The power and energy content of the imprecise ground motion acceleration may vary, even for the same soil category, affecting the complex dynamic behavior of combined structures and the vibration control capacity of secondary substructures under different frequency tuning conditions. The main purpose of this study is to develop a framework for investigating both the influence of epistemic uncertainties in the loading model and the interaction effects between the subsystems on the seismic performance of combined primary-secondary structures. To this aim, the stochastic analysis of combined structures under imprecise ground motion acceleration is addressed in both the frequency and time domains by an efficient approach capable of decoupling the propagation of interval and random uncertainties. Seismic safety assessment is performed in the framework of the *first-passage* theory by interval extension.

1. Introduction

Defining accurate models of environmental excitations, such as earthquakes or wind loads, is a crucial issue in assessing the safety of structural systems. The well-established stochastic process model is able to capture the inherent randomness of time-varying loads due to natural phenomena. The definition of suitable *Power Spectral Density* (*PSD*) functions allows the characterization of stochastic processes in the frequency domain. The non-stationary character, typical of environmental processes, can be captured by *Evolutionary Power Spectral Density* (*EPSD*) functions which describe the change of the frequency content in time. Based on the knowledge of the *PSD* or *EPSD* functions, the generation of artificial time signals can be performed using the spectral representation method [1,2]. Such artificial samples of the excitation can be used to perform reliability analysis by classical Monte Carlo Simulation (MCS) [3,4] or advanced sampling techniques [5]. The accuracy of simulation-based assessment of structural reliability is significantly affected by the ability of artificial time signals to reproduce actual records of the natural excitation.

Besides their inherently random character, environmental excitation models are affected by epistemic uncertainties due to the complexity of the underlying natural phenomena as well as measurement errors, limited or missing data, etc. To obtain reliable predictions of structural behavior, such uncertainties need to be considered in power spectrum estimates. Two pioneering studies by Vanmarcke and Lai [6], and Luco [7] have highlighted uncertainties affecting the main parameters of strong ground motions. By analyzing 140 accelerograms recorded in Western United States, Lai [8] computed the histograms of the main parameters of the Kanai-Tajimi *PSD* function and fitted them with analytical probability density functions. More recently, some approaches for estimating the *PSD* and *EPSD* function taking into account uncertainties in the data records have been proposed. The issue of quantifying the uncertainty in power spectrum estimates under missing data has been addressed, among others, by Comerford et al. [9,10] and

* Corresponding author.
E-mail addresses: alba.sofi@unirc.it (A. Sofi), federica.genovese@unirc.it (F. Genovese).

https://doi.org/10.1016/j.engstruct.2024.118885
Received 6 April 2024; Received in revised form 31 July 2024; Accepted 26 August 2024
Available online 30 September 2024

Zhang et al. [11]. Muscolino et al. [12] proposed an imprecise model of ground motion acceleration characterized by a *PSD* function depending on three interval parameters whose bounds were estimated by analyzing a set of accelerograms recorded on rigid soil deposits. Bounds for the physical parameters of an analytical *PSD* function were determined in Ref. [13] by applying a data-driven bootstrapping approach. Based on the statistical information extracted from a large data set of similar signals, Behrendt et al. [14] derived a relaxed *PSD* function utilizing subjective probabilities to capture the epistemic uncertainties. This approach was extended to non-stationary processes by defining a novel class of stochastic *EPSD* functions [15]. By using a radial basis function network, Behrendt et al. [16] proposed an imprecise *PSD* function which is able to provide optimal bounds for a set of limited data records.

Epistemic uncertainties in the loading model may significantly affect the performance of structural systems (see e.g., [12]). Response analysis under imprecise stochastic excitation is of particular relevance for combined primary-secondary systems due to their complex dynamic behavior. Indeed, interaction effects, mainly depending on the mass ratio, stiffness ratio, coupling stiffness, and frequency tuning between the subsystems (see e.g., [17–20]), may be influenced by the imprecision of the stochastic excitation. Secondary subsystems such as façades, commonly connected to primary structures for esthetic, thermal, and energy-saving purposes, are attracting increasing attention due to their vibration control capacity under environmental excitations, e.g., earthquakes and wind loads, impacts, or explosions. Relying on the classical Tuned Mass Damper (TMD) concept [21], Moon [22,23] first investigated the potential of double-skin façades (DSF) to act as vertically distributed mass dampers for multi-storey buildings under wind loads. By enabling movements of the outer façade skin via actuators, Fu and Zhang [24] proposed an integrated system that combines DSFs and mass dampers to improve building safety and energy efficiency with no need to add extra mass to the structure. Bedon and Amadio [25,26] explored the feasibility and potential of passive control systems consisting of glazing curtain walls and special mechanical connectors able to act as dissipative supports mitigating the effects of seismic loads and blast events. Recently, Pipitone et al. developed novel approaches to optimize the design of DSFs for the passive control of seismic-induced vibrations within a deterministic [27] and stochastic framework [28]. The performance of buildings with monolithic moving façades under harmonic excitation acting on the cladding system has been investigated in Ref. [29] relying on a simplified two degrees-of-freedom model. To the best of the authors' knowledge, the influence of the imprecise nature of environmental loads on the dynamic behavior of primary structures combined with secondary subsystems, e.g. façades, has not been investigated in the literature.

The present study addresses the performance assessment of combined primary-secondary structures subjected to imprecise seismic excitation. To this aim, within the *strong motion* duration, ground motion acceleration is modeled as a zero-mean stationary Gaussian random process, characterized by the interval-valued *PSD* function recently proposed in Ref. [12]. The dynamic analysis of combined structural systems under imprecise stochastic excitation is quite challenging since it involves the propagation of hybrid uncertainty i.e., interval and random, as well as the assessment of the interaction effects between the subsystems. Under the condition that the effects of aleatoric and epistemic uncertainty are kept separated [30], the propagation of hybrid uncertainty is usually performed by solving a double-loop problem. This approach requires tremendous computational effort and becomes quickly unfeasible for real-world engineering problems. Indeed, an interval *PSD* function defines a set of zero-mean stationary Gaussian random processes, one for each realization of the interval spectral parameters [31]. In this context, the application of classical MCS requires the generation of a sufficiently large number of samples for each random process belonging to the set defined by the interval *PSD* function. To enhance computational efficiency, surrogate modeling or decoupling techniques are needed. In the literature, several efficient numerical schemes for the joint propagation of epistemic and aleatoric uncertainties have been developed, such as the approaches based on advanced line sampling [32], Extended Monte Carlo simulation [33], Non-intrusive Imprecise Stochastic Simulation [34], Bayesian probabilistic propagation [35], operator norm theory [30,36,37], etc. A comprehensive overview of this topic is provided in [38,39].

In the present paper, both frequency- and time-domain formulations for the dynamic analysis of combined systems under imprecise seismic excitation are derived. A main feature of the adopted imprecise *PSD* function is the dependency on three interval parameters only. An efficient approach to carry out MCS is proposed by assuming the variance of the selected response quantity as a performance indicator. To assess the safety level of the combined structure under imprecise stochastic excitation, interval reliability analysis is performed within the framework of the classical *first-passage* problem (see e.g., [40,41]). The main purpose of the present study is to investigate the interaction effects between the subsystems and the influence of epistemic uncertainties in the loading model for different values of selected structural parameters. Due to imprecision, seismic excitation may exhibit the major power content over a wide range of frequencies [12], leading to significant changes in the performance of the coupled system, which in turn depends on the interaction effects between the subsystems.

The presented framework is applied to a six-storey shear-type frame connected by elastic springs to two independent lumped mass subsystems, subjected to imprecise ground motion acceleration.

The rest of the paper is organized as follows: in Section 2, the equations of motion of the combined primary-secondary structure are derived and the assumed model of the imprecise seismic excitation is outlined; Section 3 presents the frequency- and time-domain formulations for the dynamic analysis of the combined system under imprecise ground motion acceleration; in Section 4, seismic performance assessment is addressed within the framework of the *first-passage* theory by interval extension; in Section 5, numerical results are presented and discussed; finally, in Section 6, some concluding remarks are given.

2. Problem formulation

2.1. Equations of motion

Let us consider the combined primary-secondary system sketched in Fig. 1 [27,28]. The primary subsystem (p) is a multistorey building, modeled as a n_p − storey shear-type frame with floors characterized by equal mass m_p, lateral stiffness k_p, and interstorey height h. The viscous damping ratio ζ_p is assumed the same for all vibration modes of the building.

The lateral displacements $U_{pj}(t)$, $\left(j = 1, 2, \ldots, n_p\right)$, are the dynamically significant degrees-of-freedom (DOFs) collected into the vector $\mathbf{U}_p(t)$. The primary structure is connected at each floor by elastic springs to N independent secondary subsystems (s) consisting of elastic beam-like systems with equally spaced lumped masses m_{si}. The i−th mass has two DOFs i.e., the lateral displacement $U_{si}(t)$ and the rotation $\varphi_{si}(t)$. The secondary subsystems may be viewed as external substructures, e.g., panels of double-skin façades (see e.g., [27,28]). It is worth mentioning that the developments presented in this paper hold for different types of combined primary-secondary structures.

After static condensation of the rotational DOFs of the secondary subsystems, the n dynamically significant DOFs of the coupled system can be collected into the $n-$vector $\mathbf{U}(t) = \left[\mathbf{U}_p^T(t) \quad \mathbf{U}_{s1}^T(t) \quad \ldots. \quad \mathbf{U}_{sN}^T(t)\right]^T$, where $\mathbf{U}_{si}(t)$ is the sub-vector listing the n_{si} $(i = 1, 2, \ldots, N)$ horizontal translations of the masses of the i−th secondary subsystem $(n = n_p + n_{s1} + \ldots + n_{sN} = n_p + n_s)$; the superscript T denotes the transpose operator.

The equations of motion of the coupled system subjected to ground motion acceleration $\ddot{U}_g(t)$ (see Fig. 1) can be written in the following form:

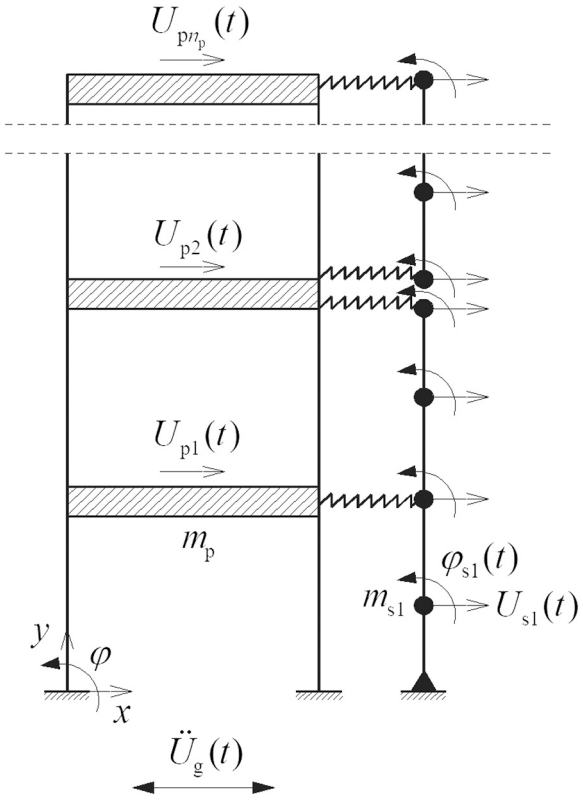

Fig. 1. Combined primary-secondary system under seismic excitation.

$$\mathbf{M}\ddot{\mathbf{U}}(t)+\mathbf{C}\dot{\mathbf{U}}(t)+\mathbf{K}\mathbf{U}(t)=-\mathbf{M}\boldsymbol{\tau}\ddot{U}_g(t) \tag{1}$$

where a dot over a variable denotes differentiation with respect to time t; $\boldsymbol{\tau}$ is the $n-$ vector listing the influence coefficients; $\mathbf{M}$ and $\mathbf{K}$ are the $n\times n$ mass and stiffness matrices of the coupled system which can be defined as follows:

$$\mathbf{M}=\begin{bmatrix}\mathbf{M}_p & \mathbf{0} & \dots & \mathbf{0}\\ \mathbf{0} & \mathbf{M}_{s1} & \dots & \mathbf{0}\\ \vdots & \vdots & \ddots & \vdots\\ \mathbf{0} & \mathbf{0} & \dots & \mathbf{M}_{sN}\end{bmatrix};\qquad \mathbf{K}=\begin{bmatrix}\mathbf{K}_p+\mathbf{K}_0 & \mathbf{K}_{sp1} & \dots & \mathbf{K}_{spN}\\ \mathbf{K}_{sp1}^{T} & \mathbf{K}_{s1} & \dots & \mathbf{0}\\ \vdots & \vdots & \ddots & \vdots\\ \mathbf{K}_{spN}^{T} & \mathbf{0} & \dots & \mathbf{K}_{sN}\end{bmatrix} \tag{2a,b}$$

where $\mathbf{M}_p$ and $\mathbf{K}_p$ are the mass and stiffness matrices of the primary structure; $\mathbf{M}_{si}$ and $\mathbf{K}_{si}$ $(i=1,2,\dots,N)$ are the mass and stiffness matrices (after static condensation) of the $i-$ th secondary subsystem; the matrix $\mathbf{K}_0$ represents the increment of the stiffness matrix of the primary structure due to the secondary subsystems; $\mathbf{K}_{spi}$ $(i=1,2,\dots,N)$ denotes the physical coupling between the primary structure and the $i-$ th subsystem; $\mathbf{0}$ is a zero matrix of appropriate dimensions. The elements of both the matrices $\mathbf{K}_0$ and $\mathbf{K}_{spi}$ depend on the stiffness of the elastic springs at each storey level. Each subsystem is considered classically damped. In particular, it is assumed that the N secondary subsystems have the same viscous damping ζ_s. Relying on these assumptions, the damping matrix of the coupled system is evaluated as follows [27]:

$$\mathbf{C}=\boldsymbol{\Gamma}^{-1}\boldsymbol{\Xi}\,\boldsymbol{\Gamma}^{-T} \tag{3}$$

where $\boldsymbol{\Gamma}$ is a suitable transformation matrix, defined following the philosophy of the component-mode synthesis method [27]:

$$\boldsymbol{\Gamma}=\begin{bmatrix}\boldsymbol{\Phi}_p & \mathbf{0} & \dots & \mathbf{0}\\ \boldsymbol{\Psi}_1 & \boldsymbol{\Phi}_{s1} & \dots & \mathbf{0}\\ \vdots & \vdots & \ddots & \vdots\\ \boldsymbol{\Psi}_N & \mathbf{0} & \dots & \boldsymbol{\Phi}_{sN}\end{bmatrix} \tag{4}$$

and $\boldsymbol{\Xi}$ is given by:

$$\boldsymbol{\Xi}=\begin{bmatrix}2\zeta_p\boldsymbol{\Omega}_p & \mathbf{0} & \dots & \mathbf{0}\\ \mathbf{0} & 2\zeta_s\boldsymbol{\Omega}_{s1} & \dots & \mathbf{0}\\ \vdots & \vdots & \ddots & \vdots\\ \mathbf{0} & \mathbf{0} & \dots & 2\zeta_s\boldsymbol{\Omega}_{sN}\end{bmatrix}. \tag{5}$$

In the previous equations, $\boldsymbol{\Phi}_i$, and $\boldsymbol{\Omega}_i$ $(i=p,s1,\dots,sN)$ are the modal and spectral matrices of the $i-$ th subsystem separately taken; $\boldsymbol{\Psi}_i=-\mathbf{K}_{si}^{-1}\mathbf{K}_{spi}^{T}\boldsymbol{\Phi}_p$ $(i=1,2,\dots,N)$ is the $i-$ th influence modal matrix.

2.2. Imprecise seismic excitation

To take into account epistemic uncertainties affecting seismic excitation, within the *strong motion* duration, ground motion acceleration is modeled as a zero-mean stationary Gaussian stochastic process characterized by the following interval-valued one-sided *Power Spectral Density* (*PSD*) function [12]:

$$G_{\ddot{U}_g}^{I}(\omega)\equiv G_{\ddot{U}_g}\left(\omega;\boldsymbol{\vartheta}^{I}\right)\equiv\left(\sigma_{\ddot{U}_g}^{2}\right)^{I}\widetilde{G}_{\ddot{U}_g}\left(\omega;\widetilde{\boldsymbol{\vartheta}}^{I}\right) \tag{6}$$

where the apex I denotes interval variables [31]; $\boldsymbol{\vartheta}^{I}=\begin{bmatrix}\Omega_0^{I} & \rho_0^{I} & \left(\sigma_{\ddot{U}_g}^{2}\right)^{I}\end{bmatrix}^{T}$ is the interval vector collecting the three main parameters characterizing the *PSD* function, which are modeled as interval variables [31] i.e., the predominant circular frequency Ω_0^{I}, the circular frequency bandwidth ρ_0^{I}, and the variance $\left(\sigma_{\ddot{U}_g}^{2}\right)^{I}$ of the random process [42]; and

$$\widetilde{G}_{\ddot{U}_g}^{I}(\omega)\equiv\widetilde{G}_{\ddot{U}_g}\left(\omega;\widetilde{\boldsymbol{\vartheta}}^{I}\right)=\beta_0^{I}\left[\frac{\omega^2}{\omega^2+\left(\omega_H^{I}\right)^2}\right]\left[\frac{\left(\omega_L^{I}\right)^4}{\omega^4+\left(\omega_L^{I}\right)^4}\right]G_0^{(CP)I}(\omega) \tag{7}$$

is the interval *PSD* function of the unit variance process $\ddot{\widetilde{U}}_g^{I}(t)\equiv\ddot{\widetilde{U}}_g\left(t;\widetilde{\boldsymbol{\vartheta}}^{I}\right)=\ddot{U}_g\left(t;\boldsymbol{\vartheta}^{I}\right)/\sigma_{\ddot{U}_g}^{I}$ with $\widetilde{\boldsymbol{\vartheta}}^{I}=\begin{bmatrix}\Omega_0^{I} & \rho_0^{I}\end{bmatrix}^{T}$ collecting only two interval spectral parameters, such that $\boldsymbol{\vartheta}^{I}=\begin{bmatrix}\widetilde{\boldsymbol{\vartheta}}^{I} & \left(\sigma_{\ddot{U}_g}^{2}\right)^{I}\end{bmatrix}^{T}$. Furthermore, in Eq. (7) $G_0^{(CP)I}(\omega)$ is the interval extension of the Conte and Peng *PSD* function [43]:

$$G_0^{(CP)I}(\omega)=\frac{\rho_0^{I}}{\pi}\left[\frac{1}{\left(\rho_0^{I}\right)^2+\left(\omega+\Omega_0^{I}\right)^2}+\frac{1}{\left(\rho_0^{I}\right)^2+\left(\omega-\Omega_0^{I}\right)^2}\right] \tag{8}$$

and

$$\begin{aligned}&\beta_0^{I}\equiv\beta_0\left(\Omega_0^{I},\rho_0^{I}\right);\\ &\omega_H^{I}\equiv\omega_H\left(\Omega_0^{I}\right)=0.1\,\Omega_0^{I};\\ &\omega_L^{I}\equiv\omega_L\left(\Omega_0^{I},\rho_0^{I}\right)=\Omega_0^{I}+0.8\,\rho_0^{I}\end{aligned} \tag{9a-c}$$

where ω_H^{I} and ω_L^{I} are the interval control frequencies of the second-order high-pass and first-order low-pass Butterworth filters, respectively; β_0^{I} is defined in Appendix A.

By applying the *Improved Interval Analysis* via *Extra Unitary Interval* (*IIA* via *EUI*) [44], the $i-$ th interval variable $\vartheta_i^{I}=\Omega_0^{I},\rho_0^{I},\left(\sigma_{\ddot{U}_g}^{2}\right)^{I}$ is defined as follows:

$$\vartheta_i^{I}=\left[\underline{\vartheta}_i,\overline{\vartheta}_i\right]\equiv\vartheta_{\mathrm{mid},i}\left(1+\alpha_i^{I}\right)=\vartheta_{\mathrm{mid},i}\left(1+\Delta\alpha_i\,\widehat{e}_i^{I}\right) \tag{10}$$

where the symbols $\underline{\vartheta}_i=\underline{\Omega}_0,\underline{\rho}_0,\underline{\sigma}_{\ddot{U}_g}^{2}$ and $\overline{\vartheta}_i=\overline{\Omega}_0,\overline{\rho}_0,\overline{\sigma}_{\ddot{U}_g}^{2}$ denote the

Lower Bound (*LB*) and *Upper Bound* (*UB*) of the interval variable, respectively; $\alpha_i^I = [\underline{\alpha}_i, \overline{\alpha}_i]$ is a symmetric interval variable ($\underline{\alpha}_i = -\overline{\alpha}_i$) representing the dimensionless fluctuation of the $i-$ th uncertain parameter around its midpoint value; $\widehat{e}_i^I = [-1, 1]$ is the so-called *EUI* associated with the $i-$ th interval variable i.e., $\widehat{e}_i^I = \widehat{e}_{\Omega_0}^I, \widehat{e}_{\rho_0}^I, \widehat{e}_{\sigma^2_{\ddot{U}_g}}^I$; $\vartheta_{\mathrm{mid},i} = \Omega_{0,\mathrm{mid}}, \rho_{0,\mathrm{mid}}, \sigma^2_{\ddot{U}_{g,\mathrm{mid}}}$ and $\Delta\alpha_i = \Delta\alpha_{\Omega_0}, \Delta\alpha_{\rho_0}, \Delta\alpha_{\sigma^2_{\ddot{U}_g}}$ are the *midpoint value* (or mean) and the normalized *deviation amplitude* (or radius) of ϑ_i^I, given, respectively, by:

$$\vartheta_{\mathrm{mid},i} = \frac{\underline{\vartheta}_i + \overline{\vartheta}_i}{2}; \qquad \Delta\alpha_i = \frac{\Delta\vartheta_i}{\vartheta_{\mathrm{mid},i}} = \frac{\overline{\alpha}_i - \underline{\alpha}_i}{2} > 0 \tag{11a,b}$$

where $\Delta\vartheta_i = (\overline{\vartheta}_i - \underline{\vartheta}_i)/\,2$ is the *deviation amplitude* of ϑ_i^I. To guarantee positive values of the spectral parameters, the condition $\Delta\alpha_i < 1$ must always be satisfied.

The midpoint and the normalized deviation amplitudes of the three interval parameters characterizing the imprecise *PSD* function, Ω_0^I, ρ_0^I, and $(\sigma^2_{\ddot{U}_g})^I$, can be estimated by analyzing a selected set of accelerograms recorded on rigid soil deposits [12]. Specifically, for the generic accelerogram, the spectral parameters can be evaluated from the knowledge of the *total intensity*, the total number of *zero-level up-crossings*, the total number of *peaks* and the *strong motion* duration [42]. Since such quantities vary from one accelerogram to another, Muscolino et al. [12] proposed to model the spectral parameters as interval variables (see Eq. (6)). The resulting interval *PSD* function may be viewed as representative of accelerograms recorded on soils with specific geotechnical characteristics.

Let us assume that the combined primary-secondary system, described in the previous section, is subjected to ground motion acceleration characterized by the interval *PSD* function in Eq. (6). Due to the imprecision of the seismic excitation, the motion of the combined system is ruled by a set of interval ordinary differential equations, which can be written as:

$$\mathbf{M}\ddot{\mathbf{U}}^I(t) + \mathbf{C}\dot{\mathbf{U}}^I(t) + \mathbf{K}\mathbf{U}^I(t) = -\mathbf{M}\boldsymbol{\tau}\ddot{U}_g^I(t) \tag{12}$$

where $\mathbf{U}^I(t) \equiv \mathbf{U}(t;\boldsymbol{\vartheta}^I)$ is the zero-mean stationary Gaussian vector process of displacements which has an interval nature. Indeed, the solution of Eq.(12) yields a set of stochastic response processes, one for each realization of the interval parameters $\boldsymbol{\vartheta}^I$ of the *PSD* function (see Eq. (6)).

It is worth noting that Eq. (12) involves hybrid or mixed uncertainty i.e., interval and random uncertainty, whose propagation is quite challenging (see e.g., [36], [37]). A naïve approach involves the solution of a double-loop problem where a stochastic analysis has to be performed for each realization of the interval parameters $\boldsymbol{\vartheta}^I$ entering the *PSD* function (see Eq. (6)). This approach is highly time-consuming and becomes unfeasible for real-world problems.

3. Interval stochastic response process

3.1. Frequency-domain analysis

The interval zero-mean stationary Gaussian stochastic response process $\mathbf{U}^I(t)$, ruled by the equations of motion in Eq. (12), can be fully characterized in the frequency domain by the interval one-sided *PSD* function matrix, given by:

$$\mathbf{G}_{\mathbf{UU}}^I(\omega) = \mathbf{H}^*(\omega)\mathbf{p}\mathbf{p}^{\mathrm{T}}\mathbf{H}^{\mathrm{T}}(\omega)G_{\ddot{U}_g}^I(\omega) \tag{13}$$

where the asterisk means complex conjugate; $\mathbf{p} = -\mathbf{M}\boldsymbol{\tau}$; $\mathbf{H}(\omega)$ is the *frequency response function* (*FRF*) matrix, defined as:

$$\mathbf{H}(\omega) = \left[-\omega^2\mathbf{M} + \mathrm{j}\,\omega\,\mathbf{C} + \mathbf{K}\right]^{-1} \tag{14}$$

with $\mathrm{j} = \sqrt{-1}$ denoting the imaginary unit.

In view of the linear dependence of the interval *PSD* function in Eq. (6) on $(\sigma^2_{\ddot{U}_g})^I$, the variance of ground motion acceleration can be assumed equal to unity and set a posteriori. Denoting with $\widetilde{\mathbf{U}}^I(t) \equiv \widetilde{\mathbf{U}}(t;\widetilde{\boldsymbol{\vartheta}}^I) = \mathbf{U}^I(t)/\sigma_{\ddot{U}_g}^I$ the displacement vector under the unit variance seismic acceleration $\widetilde{\ddot{U}}_g^I(t) \equiv \widetilde{\ddot{U}}_g(t;\widetilde{\boldsymbol{\vartheta}}^I) = \ddot{U}_g^I(t)/\,\sigma_{\ddot{U}_g}^I$, Eq. (13) can be recast as:

$$\mathbf{G}_{\mathbf{UU}}^I(\omega) = (\sigma^2_{\ddot{U}_g})^I\,\widetilde{\mathbf{G}}_{\mathbf{UU}}^I(\omega) = (\sigma^2_{\ddot{U}_g})^I\,\mathbf{H}^*(\omega)\mathbf{p}\mathbf{p}^{\mathrm{T}}\mathbf{H}^{\mathrm{T}}(\omega)\widetilde{G}_{\ddot{U}_g}^I(\omega) \tag{15}$$

where $\widetilde{\mathbf{G}}_{\mathbf{UU}}^I(\omega)$ is the *PSD* function matrix of $\widetilde{\mathbf{U}}^I(t)$; $\widetilde{G}_{\ddot{U}_g}^I(\omega) \equiv \widetilde{G}_{\ddot{U}_g}(\omega;\widetilde{\boldsymbol{\vartheta}}^I)$ is defined in Eq. (7); and the tilde denotes quantities depending only on $\widetilde{\boldsymbol{\vartheta}}^I = \left[\Omega_0^I \quad \rho_0^I\right]^{\mathrm{T}}$.

The generic response process, $Y_h^I(t) \equiv Y_h(t;\boldsymbol{\vartheta}^I) = \mathbf{q}_h^{\mathrm{T}}\mathbf{U}^I(t)$ (e.g., displacement, strain or stress at a critical point), related to the interval displacement vector $\mathbf{U}^I(t)$ through suitable combination coefficients collected into the vector $\mathbf{q}_h$, can be characterized in the frequency domain by its interval one-sided *PSD* function, defined as follows:

$$G_{Y_hY_h}^I(\omega) = (\sigma^2_{\ddot{U}_g})^I\,\widetilde{G}_{Y_hY_h}^I(\omega) = (\sigma^2_{\ddot{U}_g})^I\mathbf{q}_h^{\mathrm{T}}\,\widetilde{\mathbf{G}}_{\mathbf{UU}}^I(\omega)\mathbf{q}_h \tag{16}$$

where $\widetilde{G}_{Y_hY_h}^I(\omega)$ is the *PSD* function of the response process $\widetilde{Y}_h^I(t) = \mathbf{q}_h^{\mathrm{T}}\widetilde{\mathbf{U}}^I(t) = Y_h^I(t)/\sigma_{\ddot{U}_g}^I$ under unit variance ground motion acceleration.

The spectral moments of $Y_h^I(t)$ can be defined by interval extension as follows:

$$\begin{aligned}\lambda_{\ell,Y_h}^I \equiv \lambda_{\ell,Y_h}(\boldsymbol{\vartheta}^I) &= \int_0^\infty \omega^\ell\, G_{Y_hY_h}^I(\omega)\mathrm{d}\omega = (\sigma^2_{\ddot{U}_g})^I\int_0^\infty \omega^\ell\,\widetilde{G}_{Y_hY_h}^I(\omega)\mathrm{d}\omega \\ &= (\sigma^2_{\ddot{U}_g})^I\,\widetilde{\lambda}_{\ell,Y_h}^I, \qquad \ell = 0,1,2,\ldots\end{aligned} \tag{17}$$

In particular, the zero- and second-order spectral moments define the interval variance of the interval random process $Y_h^I(t)$ and of its time derivative i.e., $\lambda_{0,Y_h}^I \equiv (\sigma^2_{Y_h})^I$ and $\lambda_{2,Y_h}^I \equiv (\sigma^2_{\dot{Y}_h})^I$. In Eq. (17), $\widetilde{\lambda}_{\ell,Y_h}^I \equiv \widetilde{\lambda}_{\ell,Y_h}(\widetilde{\boldsymbol{\vartheta}}^I)$, $(\ell = 0,1,2,\ldots)$, denote the spectral moments of the response process $\widetilde{Y}_h^I(t) = Y_h^I(t)/\sigma_{\ddot{U}_g}^I$.

In view of the linear dependence on the variance $(\sigma^2_{\ddot{U}_g})^I$ (see Eq. (17)), the *LB* and *UB* of the interval spectral moments λ_{ℓ,Y_h}^I, can be expressed as:

$$\begin{aligned}\underline{\lambda}_{\ell,Y_h} &\equiv \min_{\boldsymbol{\vartheta}\in\boldsymbol{\vartheta}^I}\left\{\lambda_{\ell,Y_h}(\boldsymbol{\vartheta})\right\} = \underline{\sigma}^2_{\ddot{U}_g}\,\underline{\widetilde{\lambda}}_{\ell,Y_h} = \underline{\sigma}^2_{\ddot{U}_g}\min_{\boldsymbol{\vartheta}\in\widetilde{\boldsymbol{\vartheta}}^I}\left\{\widetilde{\lambda}_{\ell,Y_h}(\widetilde{\boldsymbol{\vartheta}})\right\} \\ \overline{\lambda}_{\ell,Y_h} &\equiv \max_{\boldsymbol{\vartheta}\in\boldsymbol{\vartheta}^I}\left\{\lambda_{\ell,Y_h}(\boldsymbol{\vartheta})\right\} = \overline{\sigma}^2_{\ddot{U}_g}\,\overline{\widetilde{\lambda}}_{\ell,Y_h} = \overline{\sigma}^2_{\ddot{U}_g}\max_{\boldsymbol{\vartheta}\in\widetilde{\boldsymbol{\vartheta}}^I}\left\{\widetilde{\lambda}_{\ell,Y_h}(\widetilde{\boldsymbol{\vartheta}})\right\}, \\ &\qquad \ell = 0,1,2,\ldots\end{aligned} \tag{18}$$

where $\underline{\widetilde{\lambda}}_{\ell,Y_h}$ and $\overline{\widetilde{\lambda}}_{\ell,Y_h}$ are the bounds of the interval spectral moments $\widetilde{\lambda}_{\ell,Y_h}^I \equiv \widetilde{\lambda}_{\ell,Y_h}(\widetilde{\boldsymbol{\vartheta}}^I)$ which can be computed by performing global optimization and anti-optimization with respect to the predominant circular frequency and circular frequency bandwidth i.e., $\widetilde{\boldsymbol{\vartheta}} \in \widetilde{\boldsymbol{\vartheta}}^I = \left[\Omega_0^I \quad \rho_0^I\right]^{\mathrm{T}}$. It is worth emphasizing that the combinations of the values of the parameters $\Omega_0 \in \Omega_0^I$ and $\rho_0 \in \rho_0^I$ which yield the bounds of the interval spectral moments $\widetilde{\lambda}_{\ell,Y_h}^I$ depend on the dynamic behavior of the combined structure under seismic excitation [12]. As known, such behavior is quite complex and mainly depends on the mass ratio, stiffness ratio, and link stiffness between the primary and secondary subsystems as well as

on the frequency tuning. Furthermore, resonance with some vibration modes of the structure may occur as the interval predominant circular frequency Ω_0^I varies within its range [12].

3.2. Time-domain analysis

The combined primary-secondary system is non-classically damped. To perform the time-domain dynamic analysis of the initially quiescent combined structure under imprecise seismic excitation, first, the equations of motion in Eq. (12) are rewritten in terms of state variables:

$$\dot{\mathbf{Z}}^I(t) = \mathbf{D}\,\mathbf{Z}^I(t) + \mathbf{w}\,\ddot{U}_g^I(t) \tag{19}$$

where $\mathbf{Z}^I(t)$ is the interval $2n-$ vector of state variables, $\mathbf{D}$ is a $2n \times 2n$ matrix, and $\mathbf{w}$ is a $2n-$ vector, defined, respectively, as:

$$\mathbf{Z}^I(t) = \begin{bmatrix} \mathbf{U}^I(t) \\ \dot{\mathbf{U}}^I(t) \end{bmatrix}; \qquad \mathbf{D} = \begin{bmatrix} \mathbf{0} & \mathbf{I}_n \\ -\mathbf{M}^{-1}\mathbf{K} & -\mathbf{M}^{-1}\mathbf{C} \end{bmatrix}; \qquad \mathbf{w} = \begin{bmatrix} \mathbf{0} \\ -\boldsymbol{\tau} \end{bmatrix} \tag{20a-c}$$

with $\mathbf{I}_n$ denoting the $n-$ order identity matrix.

The solution of Eq. (19) under zero initial conditions at $t_0 = 0$ can be expressed in the following integral form [45,46]:

$$\mathbf{Z}^I(t) = \int_{t_0}^{t} \boldsymbol{\Theta}(t-\tau)\mathbf{w}\ddot{U}_g^I(\tau)\mathrm{d}\tau \tag{21}$$

where $\boldsymbol{\Theta}(t)$ is the *transition matrix* which can be evaluated as follows:

$$\boldsymbol{\Theta}(t) = \exp(\mathbf{D}t) = \boldsymbol{\Upsilon}\exp(\boldsymbol{\Lambda}t)\boldsymbol{\Upsilon}^{\mathrm{T}}\mathbf{A} = \boldsymbol{\Upsilon}^{*}\exp(\boldsymbol{\Lambda}^{*}t)\boldsymbol{\Upsilon}^{*\mathrm{T}}\mathbf{A}. \tag{22}$$

In the previous equation, $\boldsymbol{\Upsilon}$ is a complex matrix of order $(2n \times 2m)$ which collects the first $2m$ $(m \le n)$ complex eigenvectors obtained as solution of the following eigenproblem:

$$\mathbf{D}^{-1}\boldsymbol{\Upsilon} = \boldsymbol{\Upsilon}\boldsymbol{\Lambda}^{-1}; \qquad \boldsymbol{\Upsilon}^{\mathrm{T}}\mathbf{A}\boldsymbol{\Upsilon} = \mathbf{I}_{2m} \tag{23}$$

where $\boldsymbol{\Lambda}$ is a diagonal matrix collecting the first $2m$ complex eigenvalues; and

$$\mathbf{A} = \begin{bmatrix} \mathbf{C} & \mathbf{M} \\ \mathbf{M} & \mathbf{0} \end{bmatrix}. \tag{24}$$

To enhance computational efficiency, the set of interval first-order ordinary differential equations in Eq.(19) can be decoupled by employing *complex modal analysis*. To this aim, the following coordinate transformation is introduced:

$$\mathbf{Z}^I(t) = \boldsymbol{\Upsilon}\,\mathbf{X}^I(t) \tag{25}$$

where $\mathbf{X}^I(t)$ is an interval complex vector of order $2m$, with $m \le n$ denoting the number of retained complex modes.

By applying the coordinate transformation in Eq. (25), Eq. (19) yields the following set of $2m$ decoupled interval first-order ordinary differential equations with complex coefficients:

$$\dot{\mathbf{X}}^I(t) = \boldsymbol{\Lambda}\,\mathbf{X}^I(t) + \mathbf{v}\,\ddot{U}_g^I(t) \tag{26}$$

where $\mathbf{v} = \boldsymbol{\Upsilon}^{\mathrm{T}}\mathbf{A}\mathbf{w}$.

The interval statistics of the response process can be defined in the time domain by applying classical Monte Carlo Simulation (MCS). Due to imprecision of the stochastic excitation, MCS involves a double loop which requires a tremendous computational burden. Indeed, for each realization of the interval spectral parameters $\boldsymbol{\vartheta}^I = \left[\Omega_0^I \quad \rho_0^I \quad (\sigma_{\ddot{U}_g}^2)^I\right]^{\mathrm{T}}$, N_G samples of the associated stochastic excitation need to be generated. By applying the classical spectral representation [1], the $k-$ th sample of the imprecise ground motion acceleration, associated with the $j-$ th realization of the epistemic uncertainties $\boldsymbol{\vartheta}^{(j)}$, reads:

$$\ddot{U}_g^{(k)}(t;\boldsymbol{\vartheta}^{(j)}) = \sum_{i=1}^{M} \sqrt{2\,G_{\ddot{U}_g}(\omega_i;\boldsymbol{\vartheta}^{(j)})\Delta\omega}\,\sin\left(\omega_i t + \phi_i^{(k)}\right) \tag{27}$$

where $\phi_i^{(k)}$ are M independent random phases uniformly distributed in the interval $[0, 2\pi]$; $\Delta\omega$ is a constant step along the frequency axis, and $\omega_i = i\Delta\omega$.

For each sample of the imprecise seismic excitation, the associated sample of structural response can be obtained by the step-by-step integration of Eq. (26) (see Appendix B).

The computational effort increases with the number of samples and becomes unfeasible for real-world structures. Suitable strategies are needed to enhance computational efficiency. This issue is addressed in the next section.

4. Safety assessment under imprecise seismic excitation

Safety assessment of the combined structure under imprecise seismic excitation can be performed by interval extension of the *first-passage* theory (see e.g., [40,41]).

Due to epistemic uncertainties affecting the *PSD* function of ground motion acceleration, the *extreme value* random process, over the time interval $[0, T]$, for the generic response process $Y_h^I(t)$ has an interval nature and is defined as:

$$Y_{h,\max}^I(T) \equiv Y_{h,\max}(T;\boldsymbol{\vartheta}^I) = \max_{0\le t\le T}\left|Y_h(t;\boldsymbol{\vartheta}^I)\right| \tag{28}$$

where the symbol $|\bullet|$ denotes absolute value.

The safety condition can be established by evaluating the probability that $Y_{h,\max}^I(T)$ is equal to or less than a critical level b within the time interval $[0, T]$ i.e., estimating the so-called interval *cumulative distribution function* (*CDF*) or interval *reliability function*, $L_{Y_{h,\max}}^I(b,T)$, of the *extreme value* random process. As known, the evaluation of such a function is quite challenging, even when no epistemic uncertainties affecting the stochastic excitation are considered.

An approximate expression of the interval *CDF* can be obtained by interval extension of Vanmarcke's *first-passage* failure criterion [47] i.e.:

$$\begin{aligned} L_{Y_{h,\max}}^I(b,T) &\equiv L_{Y_{h,\max}}(b,T;\boldsymbol{\vartheta}^I) = \Pr\left[Y_{h,\max}^I(T) \le b\right] \\ &\cong \exp\left[-\frac{T}{\pi}\sqrt{\frac{\widetilde{\lambda}_{2,Y_h}^I}{\widetilde{\lambda}_{0,Y_h}^I}}\left[\frac{1-\exp\left(-b\,(\widetilde{\delta}_{Y_h}^I)^{1.2}\sqrt{\dfrac{\pi}{2\,(\sigma_{\ddot{U}_g}^2)^I\,\widetilde{\lambda}_{0,Y_h}^I}}\right)}{\exp\left(\dfrac{b^2}{2\,(\sigma_{\ddot{U}_g}^2)^I\,\widetilde{\lambda}_{0,Y_h}^I}\right)-1}\right]\right] \end{aligned} \tag{29}$$

where

$$\widetilde{\delta}_{Y_h}^I \equiv \widetilde{\delta}_{Y_h}(\widetilde{\boldsymbol{\vartheta}}^I) = \sqrt{1 - \frac{\mathrm{Re}\left\{\widetilde{\lambda}_{1,Y_h}^I\right\}^2}{\widetilde{\lambda}_{0,Y_h}^I\,\widetilde{\lambda}_{2,Y_h}^I}} \tag{30}$$

is the so-called interval bandwidth parameter of the response process $\widetilde{Y}_h^I(t) = Y_h^I(t)/\sigma_{\ddot{U}_g}^I$.

Approximate estimates of the *LB* and *UB* of the interval *CDF* can be efficiently obtained relying on the knowledge of the bounds of the spectral moments $\widetilde{\lambda}_{\ell,Y_h}^I, (\ell = 0,1,2)$, (see Eqs. (18)) as follows [12]:

$$\underline{L}_{Y_{h,\max}}(b,T) \equiv \min_{\mathfrak{\vartheta}\in\mathfrak{\vartheta}^I}\left\{L_{Y_{h,\max}}(b,T;\,\mathfrak{\vartheta})\right\} \approx L_{Y_{h,\max}}\left(b,T;\;\overline{\sigma}^2_{\ddot{U}_g},\overline{\overline{\lambda}}_{0,Y_h},\overline{\overline{\lambda}}_{1,Y_h},\overline{\overline{\lambda}}_{2,Y_h}\right);$$
$$\overline{L}_{Y_{h,\max}}(b,T) \equiv \max_{\mathfrak{\vartheta}\in\mathfrak{\vartheta}^I}\left\{L_{Y_{h,\max}}(b,T;\,\mathfrak{\vartheta})\right\} \approx L_{Y_{h,\max}}\left(b,T;\;\underline{\sigma}^2_{\ddot{U}_g},\underline{\widetilde{\lambda}}_{0,Y_h},\underline{\widetilde{\lambda}}_{1,Y_h},\underline{\widetilde{\lambda}}_{2,Y_h}\right). \tag{31a,b}$$

The previous relationships allow one to avoid the time-consuming solution of a global optimization and anti-optimization problem for each value of the barrier level b.

Taking into account that the zero-order spectral moment $\lambda^I_{0,Y_h} \equiv (\sigma^2_{Y_h})^I$ has the highest impact on reliability (see e.g., [12,30]), the following approximate expressions of the bounds of the interval *CDF* are proposed:

$$\underline{L}_{Y_{h,\max}}(b,T) \approx L_{Y_{h,\max}}\left(b,T;\;\mathfrak{\vartheta}^{(UB)}\right);$$
$$\overline{L}_{Y_{h,\max}}(b,T) \approx L_{Y_{h,\max}}\left(b,T;\;\mathfrak{\vartheta}^{(LB)}\right) \tag{32a,b}$$

where the quantities $\mathfrak{\vartheta}^{(UB)} = \left[\Omega_0^{(UB)} \quad \rho_0^{(UB)} \quad (\sigma^2_{\ddot{U}_g})^{(UB)}\right]^{\mathrm{T}}$ and $\mathfrak{\vartheta}^{(LB)} = \left[\Omega_0^{(LB)} \quad \rho_0^{(LB)} \quad (\sigma^2_{\ddot{U}_g})^{(LB)}\right]^{\mathrm{T}}$, with $(\sigma^2_{\ddot{U}_g})^{(UB)} = \overline{\sigma}^2_{\ddot{U}_g}$ and $(\sigma^2_{\ddot{U}_g})^{(LB)} = \underline{\sigma}^2_{\ddot{U}_g}$, are the realizations of the interval vector $\mathfrak{\vartheta}^I = \left[\Omega_0^I \quad \rho_0^I \quad (\sigma^2_{\ddot{U}_g})^I\right]^{\mathrm{T}}$ which characterize the seismic excitation leading to the *UB* and *LB* of the interval variance $\lambda^I_{0,Y_h} \equiv (\sigma^2_{Y_h})^I$ of the selected response process, respectively.

Based on the knowledge of the *LB* and *UB* of the interval *reliability function*, the bounds of the interval *failure probability function* $P^I_{f,Y_{h,\max}}(b,T) \equiv P_{f,Y_{h,\max}}\left(b,T;\mathfrak{\vartheta}^I\right)$ can be derived as follows:

$$\underline{P}_{f,Y_{h,\max}}(b,T) = 1 - \overline{L}_{Y_{h,\max}}(b,T);$$
$$\overline{P}_{f,Y_{h,\max}}(b,T) = 1 - \underline{L}_{Y_{h,\max}}(b,T). \tag{33a,b}$$

It is worth emphasizing that the *LB* of the interval *CDF* and the associated *UB* of the interval *failure probability* (Eqs. (32a) and (33b)), identify the worst-case scenario and correspond to the realization of the interval *PSD* with $\mathfrak{\vartheta} = \mathfrak{\vartheta}^{(UB)}$. Based on this observation, within the family of stochastic processes defined by the interval *PSD* function in Eq. (6), the critical seismic excitation, leading to the worst-case scenario, may be identified as the one pertaining to the combination of the interval spectral parameters $\mathfrak{\vartheta}^{(c)} \equiv \mathfrak{\vartheta}^{(UB)} = \left[\Omega_0^{(UB)} \quad \rho_0^{(UB)} \quad \overline{\sigma}^2_{\ddot{U}_g}\right]^{\mathrm{T}}$, which yields the *UB* of the variance of the selected response process $\overline{\lambda}_{0,Y_h} = \overline{\sigma}^2_{\ddot{U}_g}\,\overline{\overline{\lambda}}_{0,Y_h} \equiv \overline{\sigma}^2_{Y_h}$. Once the critical excitation has been identified, MCS can be efficiently performed by generating N_G samples of the zero-mean stationary Gaussian random process $\ddot{U}_g\left(t;\mathfrak{\vartheta}^{(c)}\right)$, characterized by the one-sided *PSD* function $G_{\ddot{U}_g}\left(\omega;\mathfrak{\vartheta}^{(c)}\right)$.

A notable feature of the proposed approach is the capability of decoupling the propagation of interval and random uncertainties by assuming the variance of the response as a performance indicator. Thus, the time-consuming double loop can be avoided in both the frequency and time domain. The presented formulation can be applied to investigate the performance of combined primary-secondary structures, like the one shown in Fig. 1, under imprecise seismic excitation. In particular, the influence of epistemic uncertainties on the vibration control capacity of the secondary subsystems is of interest for design purposes (see e.g., [27,28]).

5. Numerical application

The six-storey shear-type frame (primary subsystem) coupled with two independent beam-like structures with equally spaced lumped masses m_{si} (secondary subsystem), shown in Fig. 2, is considered as a case study [27,28]. The subsystems are connected to the shear-type frame by means of elastic springs at the floor level. The primary subsystem is characterized by the following parameters: floor mass $m_p = 20000$ kg; lateral stiffness $k_p = 4 \times 10^7$ N/m; interstorey height $h = 3.3$ m; and viscous damping ratio $\zeta_p = 0.02$. The fundamental period of vibration of the primary structure is $T_{p0} = 0.582$ s.

The secondary substructures may be viewed as two independent panels whose total mass is assumed equal to 10 % of the mass of the primary building. Each lumped mass m_{si} is assumed to account for half the interstorey mass of the secondary subsystem. The stiffness of the links and the flexural stiffness of each secondary subsystem are assumed proportional to the lateral stiffness of the shear-type frame k_p [27,28] through the non-dimensional coefficients η and υ, respectively, i.e., ηk_p and υk_p. When not otherwise specified, it is assumed $\upsilon = 0.6$, while different values of the parameter η within the range $\eta_{\min} \le \eta \le \eta_{\max}$, with $\eta_{\min} = 1.7 \times 10^{-3}$ and $\eta_{\max} = 5.1 \times 10^{-3}$, are considered. The viscous damping ratio of the secondary subsystems is set equal to $\zeta_s = 0.13$. The values of the main structural parameters are selected relying on Refs. [27,28].

The interval zero-mean stationary Gaussian random process describing the displacement of the first floor of the primary structure, $U^I_{p1}(t)$, is selected as the response quantity of interest. In particular, the variance of $U^I_{p1}(t)$ is assumed as performance variable and the bounds of the interval *reliability function*, $L^I_{U_{p1,\max}}(b,T)$, and interval *failure probability*, $P^I_{f,U_{p1,\max}}(b,T)$, are evaluated to assess the seismic behavior of the combined system.

The *LB* and *UB* of the interval parameters, Ω_0^I, ρ_0^I, and $(\sigma^2_{\ddot{U}_g})^I$, entering the interval *PSD* function of ground motion acceleration in Eq. (6), are estimated by analyzing a set of accelerograms that are site-compatible

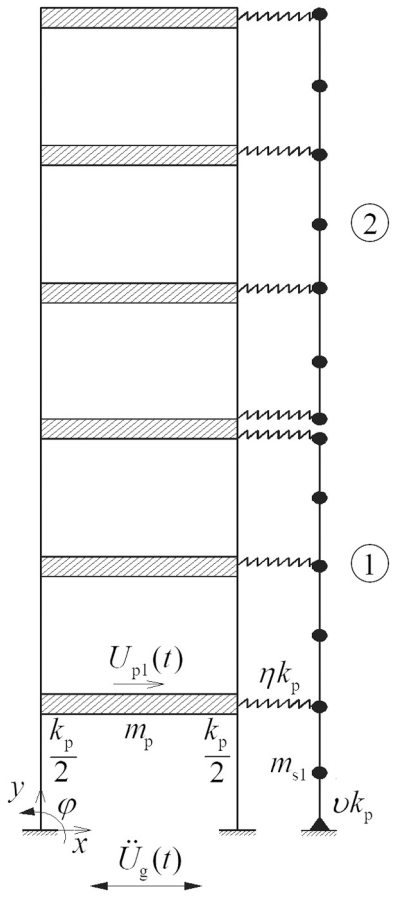

Fig. 2. Six-storey shear-type frame coupled with two secondary subsystems, subjected to imprecise earthquake ground motion.

Table 1
Main recording information on the selected accelerograms.

	Earthquake name	Component	Station name	Date
1	San Fernando	270	Pasadena - Old Seismo Lab	9/2/1971
2	Northridge−01	185	LA – Wonderland Ave	17/1/1994
3	Northridge−01	0	Vasquez Rocks Park	17/1/1994
4	Northridge−01	90	Vasquez Rocks Park	17/1/1994
5	Tottori Japan	EW	SMNH10	6/10/2000
6	Central Italy	HE	Accumoli	30/10/2016
7	Central Italy	HGN	Accumoli	30/10/2016
8	Central Italy	HNE	Avendita PG	30/10/2016
9	Central Italy	HNN	Avendita PG	30/10/2016
10	Central Italy	HNE	Savelli PG	30/10/2016

with the Port Area of Tremestieri, located in Southern Italy. This area falls in the seismogenic zone ZS929, which is part of the seismic source zone model (ZS9) used for the seismic hazard assessment of the Italian territory [48]. With reference to the Life Limit State, earthquake ground motions recorded on rock subsoil having *moment magnitude* $M_W = 6.5 \pm 0.2$ and Joyner-Boore distance [49] $R_{jb} = 0 \div 30$ km are selected. By applying these criteria, a set of 10 acceleration time histories is downloaded from the PEER [50] and ESM [51] databases (see Table 1). Subsequently, each accelerogram in the set is scaled to achieve the target peak ground acceleration value $a_g = 3.33\ \mathrm{m/s^2}$. It is worth remarking that assuming sufficiently tight ranges of key parameters, such as the *moment magnitude* and Joyner-Boore distance, is critical to obtain a realistic description of seismic acceleration which is site-compatible with a specific area.

For all the selected accelerograms, the *total intensity*, the total number of *zero-level up-crossings*, the total number of *peaks* and the *strong motion* duration are evaluated to derive the three main parameters characterizing the assumed model of the imprecise *PSD* function of seismic excitation i.e., the variance $\sigma^2_{\ddot{U}_g}$, the predominant circular frequency Ω_0, and the circular frequency bandwidth ρ_0. Then, the *LB*, *UB*, midpoint (mid), and the normalized deviation amplitude (dev/mid) of the three spectral parameters listed in Table 2 are obtained.

In order to investigate the dynamic behavior of the combined primary-secondary system in the frequency domain, in Fig. 3 the modulus of the *FRF* for the first-floor displacement of the primary structure (i.e., the first element of the vector $|\mathbf{H}(\omega)\mathbf{p}|$), obtained considering different values of the link stiffness ηk_p, is compared with the one pertaining to the primary structure separately taken. In particular, the dynamic behavior for the assumed minimum and maximum values of the link stiffness parameter η, $\eta_{\min}$ and $\eta_{\max}$, as well as for an intermediate value $\widehat{\eta} = 3.7 \times 10^{-3}$ is scrutinized. It can be observed that the *FRF* is significantly affected by the stiffness of the links between the primary and the secondary subsystems. Interestingly, when the non-dimensional link stiffness parameter is set equal to $\widehat{\eta}$, the *FRF* exhibits two distinct peaks in place of the first modal peak. A similar feature typically characterizes the frequency-domain behavior in the presence of a traditional TMD. When the maximum value of the link stiffness is considered i.e., $\eta = \eta_{\max}$, the first modal peak of the combined structure is shifted to the left and its height is reduced compared to the one of the primary structure.

Fig. 4 shows the variance $\widetilde{\lambda}^I_{0,U_{p1}} \equiv (\widetilde{\sigma}^2_{U_{p1}})^I$ of the interval stochastic process $\widetilde{U}^I_{p1}(t) = U^I_{p1}(t)/\sigma^I_{\ddot{U}_g}$ (see Eq. (17)), for $\eta = \widehat{\eta}$ and $\upsilon = 0.6$, versus the predominant circular frequency $\Omega_0 \in \Omega^I_0$ and circular frequency bandwidth $\rho_0 \in \rho^I_0$ of seismic acceleration (see Table 2). It can be observed that the variance $\widetilde{\lambda}^I_{0,U_{p1}} \equiv (\widetilde{\sigma}^2_{U_{p1}})^I$ is a monotonic decreasing function of the predominant circular frequency. Thus, the *LB* and *UB* of $\widetilde{\lambda}^I_{0,U_{p1}} \equiv (\widetilde{\sigma}^2_{U_{p1}})^I$ are achieved when the predominant circular frequency is set equal to its *UB* and *LB*, respectively, i.e. $\Omega_0^{(LB)} = \overline{\Omega}_0$ and $\Omega_0^{(UB)} = \underline{\Omega}_0$. Furthermore, the *LB* and *UB* of the variance of the response process $\widetilde{U}^I_{p1}(t)$ are attained when the circular frequency bandwidth is equal to its *LB*, $\rho_0^{(LB)} = \underline{\rho}_0$, and to the intermediate value $\rho_0^{(UB)} = 19.42$ rad/s, respectively. Therefore, the vectors collecting the values of the interval predominant circular frequency and circular frequency bandwidth which yield the *LB* and *UB* of $\widetilde{\lambda}^I_{0,U_{p1}} \equiv (\widetilde{\sigma}^2_{U_{p1}})^I$ are defined as $\widetilde{\boldsymbol{\vartheta}}^{(LB)} = \begin{bmatrix} \overline{\Omega}_0 & \underline{\rho}_0 \end{bmatrix}^{\mathrm{T}}$ and $\widetilde{\boldsymbol{\vartheta}}^{(UB)} = \begin{bmatrix} \underline{\Omega}_0 & \rho_0^{(UB)} \end{bmatrix}^{\mathrm{T}}$ with $\rho_0^{(UB)} = 19.42$ rad/s, respectively.

Table 2
Main characteristics of the interval spectral parameters.

Parameter	*LB*	*UB*	mid	dev/mid
$\sigma^2_{\ddot{U}_g}\left[\mathrm{m^2/s^4}\right]$	0.64	1.47	1.06	0.39
Ω_0[rad/s]	23.91	45.22	34.57	0.31
ρ_0[rad/s]	12.10	22.56	17.33	0.30

When dealing with imprecise stochastic excitations, a key issue to be investigated is the potential occurrence of resonance conditions with some structural vibration modes. For the selected case study, no resonance with the first vibration mode of the coupled structure may occur as the predominant circular frequency of the excitation varies within the pertinent interval (see Table 2) and the stiffness parameters, υ and η, range between the prescribed limits.

Fig. 5 displays the realizations of the interval *PSD* function $\widetilde{G}^I_{\ddot{U}_g}(\omega)$ (see Eq. (7)) of the unit variance seismic acceleration for assigned values of the interval spectral parameters Ω^I_0 and ρ^I_0, including the midpoints $\widetilde{\boldsymbol{\vartheta}}_{\mathrm{mid}} = \begin{bmatrix} \Omega_{0,\mathrm{mid}} & \rho_{0,\mathrm{mid}} \end{bmatrix}^{\mathrm{T}}$ and those giving the *LB* and *UB* of $\widetilde{\lambda}^I_{0,U_{p1}} \equiv (\widetilde{\sigma}^2_{U_{p1}})^I$ i.e., $\widetilde{\boldsymbol{\vartheta}}^{(LB)} = \begin{bmatrix} \overline{\Omega}_0 & \underline{\rho}_0 \end{bmatrix}^{\mathrm{T}}$ and $\widetilde{\boldsymbol{\vartheta}}^{(UB)} = \begin{bmatrix} \underline{\Omega}_0 & \rho_0^{(UB)} \end{bmatrix}^{\mathrm{T}}$. It can be observed that, due to epistemic uncertainties affecting the spectral parameters, the actual *PSD* function of ground motion acceleration may exhibit the major power content over a broad range of frequencies, leading to different dynamic behaviors of the seismically excited structure.

The *LB* and *UB* of the variance of the interval random response process $U^I_{p1}(t) = \sigma^I_{\ddot{U}_g}\widetilde{U}^I_{p1}(t)$ are achieved when $\widetilde{\boldsymbol{\vartheta}} = \widetilde{\boldsymbol{\vartheta}}^{(LB)}$ and $\widetilde{\boldsymbol{\vartheta}} = \widetilde{\boldsymbol{\vartheta}}^{(UB)}$, respectively, and the interval variance of the imprecise ground motion acceleration process is equal to its *LB* and *UB* i.e., $(\sigma^2_{\ddot{U}_g})^{(LB)} = \underline{\sigma}^2_{\ddot{U}_g}$ and $(\sigma^2_{\ddot{U}_g})^{(UB)} = \overline{\sigma}^2_{\ddot{U}_g}$. Thus, the critical excitation, leading to the worst-case scenario, is characterized by the *PSD* function in Eq. (6) with the following values of the uncertain parameters:

$$\boldsymbol{\vartheta}^{(c)} \equiv \boldsymbol{\vartheta}^{(UB)} = \begin{bmatrix} \widetilde{\boldsymbol{\vartheta}}^{(UB)} & \overline{\sigma}^2_{\ddot{U}_g} \end{bmatrix}^{\mathrm{T}} = \begin{bmatrix} \underline{\Omega}_0 & \rho_0^{(UB)} & \overline{\sigma}^2_{\ddot{U}_g} \end{bmatrix}^{\mathrm{T}}.$$

To gain a deeper insight into the dynamic behavior of the combined structure under imprecise seismic excitation, in Fig. 6 the realizations of the imprecise one-sided *PSD* function $\widetilde{G}^I_{U_{p1}U_{p1}}(\omega) = G^I_{U_{p1}U_{p1}}(\omega)/(\sigma^2_{\ddot{U}_g})^I$ (see Eq. (16)) of the displacement process $\widetilde{U}^I_{p1}(t)$ pertaining to the values of the interval parameters Ω^I_0 and ρ^I_0 which yield the *LB* and *UB* of the variance $\widetilde{\lambda}^I_{0,U_{p1}} \equiv (\widetilde{\sigma}^2_{U_{p1}})^I$ i.e., $\widetilde{\boldsymbol{\vartheta}}^{(LB)}$ and $\widetilde{\boldsymbol{\vartheta}}^{(UB)}$, as well as to the nominal or midpoint values $\widetilde{\boldsymbol{\vartheta}}_{\mathrm{mid}}$ are plotted. Three different values of the link stiffness ηk_p are considered. Consistently with the frequency-domain behavior of the coupled structure disclosed by the *FRF*s in Fig. 3, it is observed that the peak associated with the first natural frequency is shifted when the connection stiffness changes, and it is replaced by two distinct peaks when $\eta = \widehat{\eta}$. For such a value of the link stiffness, the secondary substructures act like distributed vibration absorbers. Fig. 6 also shows the remarkable influence of epistemic uncertainties affecting seismic excitation on the *PSD* of structural response, in agreement with the results plotted in Fig. 4.

The stiffness of the links as well as the mass and stiffness ratio be-

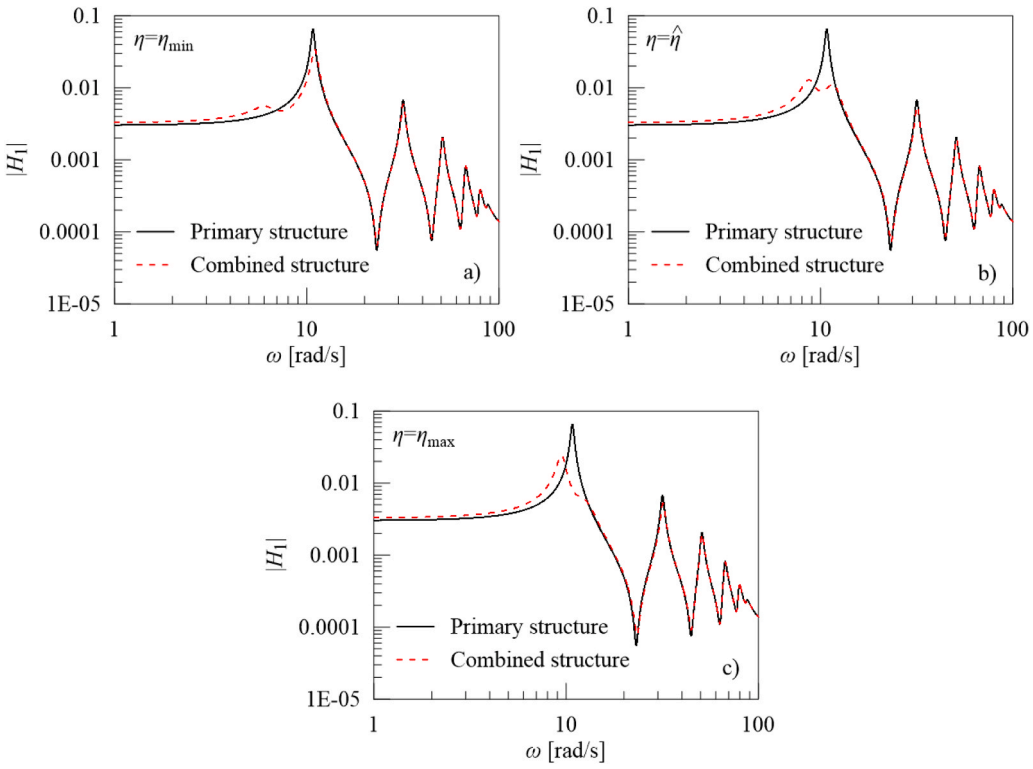

Fig. 3. Modulus of the *FRF* of the first-floor displacement of the primary subsystem compared with the one of the coupled structure for different values of the link stiffness ηk_p: a) $\eta = \eta_{min}$; b) $\eta = \hat{\eta}$; and c) $\eta = \eta_{max}$ ($\upsilon = 0.6$).

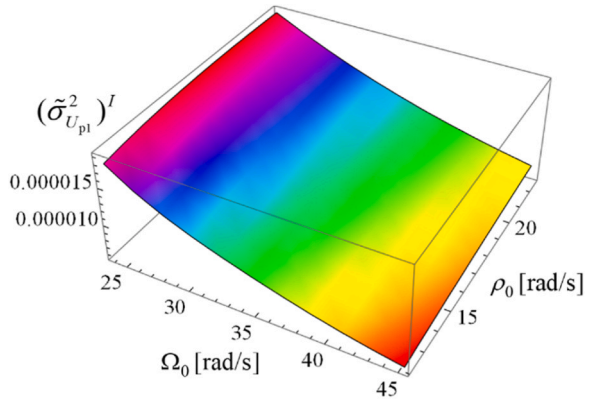

Fig. 4. Variance of the response process $\tilde{U}^I_{p1}(t)$ versus the predominant circular frequency Ω_0 and circular frequency bandwidth ρ_0 ($\eta = \hat{\eta}$, $\upsilon = 0.6$).

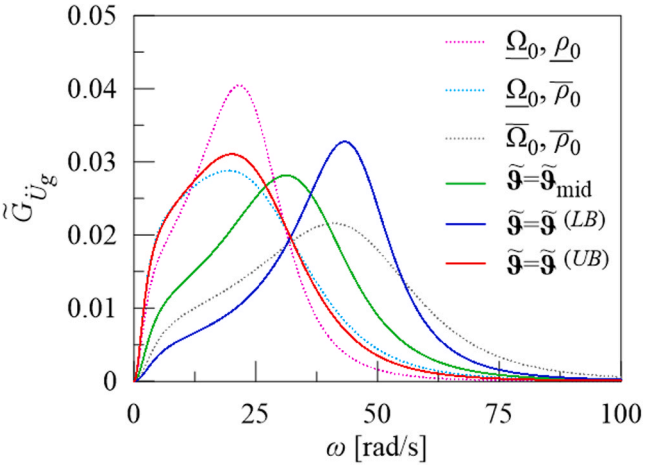

Fig. 5. Realizations of the imprecise *PSD* function $\tilde{G}^I_{\ddot{U}_g}(\omega)$ of ground motion acceleration pertaining to different values of the interval predominant circular frequency Ω^I_0 and circular frequency bandwidth ρ^I_0 collected into the interval vector $\tilde{\mathfrak{I}} = [\Omega_0 \quad \rho_0]^T$, ($\eta = \hat{\eta}$, $\upsilon = 0.6$).

tween the primary and secondary subsystems have a significant influence on the interaction effects between the subsystems. In the presence of imprecise seismic excitation, the dynamic behavior of the coupled system depends not only on the interaction between the subsystems but also on epistemic uncertainties affecting the *PSD* function of ground motion acceleration. Fig. 7 displays the *LB*, *UB*, and nominal value of the variance $\tilde{\lambda}^I_{0,U_{p1}} \equiv (\tilde{\sigma}^2_{U_{p1}})^I$ of the interval random process $\tilde{U}^I_{p1}(t)$ versus the non-dimensional link and secondary subsystem stiffness parameters η and υ. The values of the stiffness parameters which minimize the quantities plotted in Fig. 7 are nearly $\eta = \hat{\eta}$ and $\upsilon = 0.6$. Indeed, as shown in Figs. 3b and 6b, for these values of the stiffness parameters, an energy transfer from the primary to the secondary subsystems takes place and the ratios between the natural frequencies of the primary and secondary substructures are close to unity i.e., $\omega_p/\omega_{s1} = 1.01$ and $\omega_p/\omega_{s2} = 1.14$. Though the optimal design of the secondary subsystems as vibration absorbers is out of the scope of the present study, it is worth observing that the stiffness parameters minimizing the variance of the first-floor displacement are not affected by the imprecision of the seismic excitation for the selected case study. However, the range of structural performance changes significantly due to epistemic uncertainties. When secondary subsystems are conceived as retrofit solutions to reduce the vibration amplitudes of the primary structure under seismic excitation, their design should take into account the imprecision of ground motion acceleration. Indeed, the vibration control capacity of the secondary subsystems may be significantly overestimated due to epistemic uncertainties affecting seismic excitation. Fig. 7 shows that

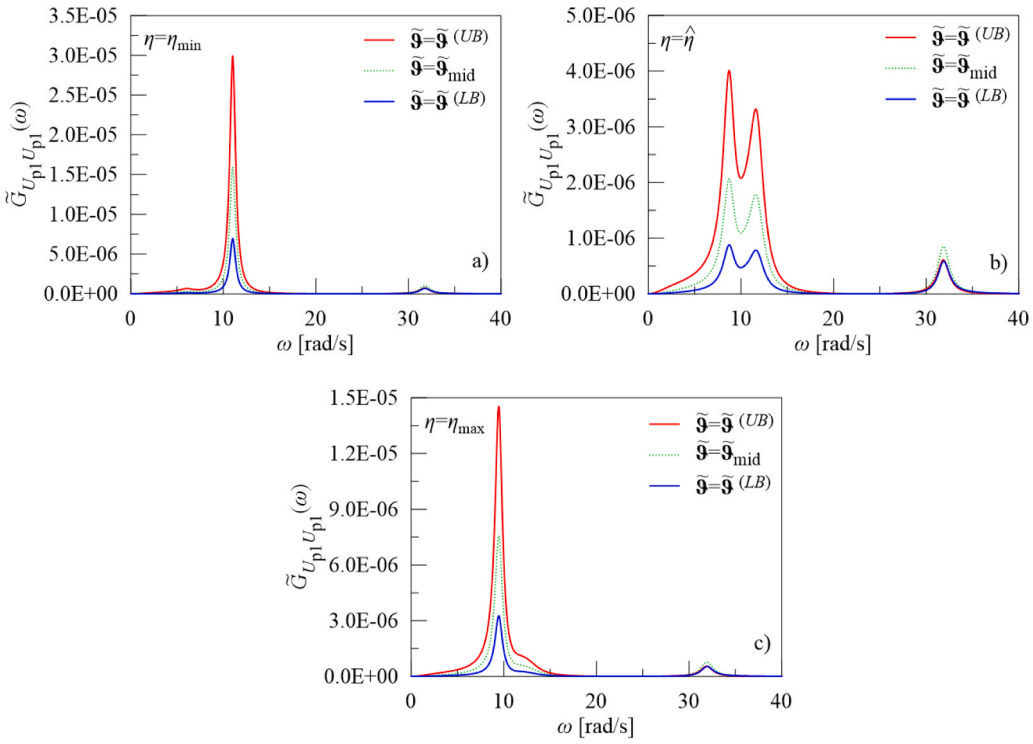

Fig. 6. Realizations of the interval one-sided *PSD* function of the response process $\widetilde{U}^I_{\mathrm{p1}}(t)$ for assigned values of the uncertain spectral parameters and different values of the link stiffness ηk_{p}: a) $\eta = \eta_{\min}$; b) $\eta = \hat{\eta}$; and c) $\eta = \eta_{\max}$ ($\upsilon = 0.6$).

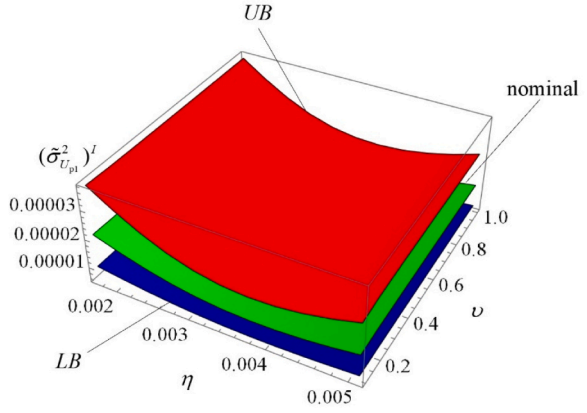

Fig. 7. *LB*, *UB*, and nominal value of the variance of the response process $\widetilde{U}^I_{\mathrm{p1}}(t)$ versus the non-dimensional link and subsystem stiffness parameters η and υ.

the stiffness of the connections between the primary and secondary subsystems affects the interval variance $\widetilde{\lambda}^I_{0,U_{\mathrm{p1}}} \equiv (\widetilde{\sigma}^2_{U_{\mathrm{p1}}})^I$ more than the stiffness of the secondary subsystems. The dependency of the *LB*, *UB*, and nominal value of the variance of the response process $\widetilde{U}^I_{\mathrm{p1}}(t)$ on the link stiffness parameter η, for assigned value of $\upsilon = 0.6$, is shown in Fig. 8.

To investigate the time-domain dynamic behavior of the combined primary-secondary structure, samples of the imprecise seismic excitation for selected realizations of the interval spectral parameters are generated by applying Eq. (27) with $M = 1000$ and $\Delta\omega = 0.1$ rad/s. The corresponding response samples are obtained by integrating Eq. (26), assuming a time step $\Delta t = 0.005$ s (Appendix B). Fig. 9 shows some samples of the interval stochastic response process $\widetilde{U}^I_{\mathrm{p1}}(t)$ for assigned values of the interval predominant circular frequency and circular frequency bandwidth of the excitation i.e., the midpoint values, $\widetilde{\mathfrak{d}}_{\mathrm{mid}}$, and the combinations which give the *LB* and *UB* of the variance, $\widetilde{\mathfrak{d}}^{(LB)}$ and $\widetilde{\mathfrak{d}}^{(UB)}$. Three different values of the connection stiffness parameter η are considered while $\upsilon = 0.6$. As expected, both the vibration amplitude and frequency content of the samples are affected by the selection of the spectral parameters. In particular, the critical excitation, identified by $\widetilde{\mathfrak{d}}^{(c)} = \widetilde{\mathfrak{d}}^{(UB)}$, causes the largest vibration amplitudes for all the considered values of the link stiffness parameter η.

To assess the vibration control capacity of the secondary subsystems, Fig. 10 displays some samples of the interval stochastic response process $\widetilde{U}^I_{\mathrm{p1}}(t)$ of the combined ($\eta = \hat{\eta}$, $\upsilon = 0.6$) and primary structure for assigned values of the interval spectral parameters i.e., $\widetilde{\mathfrak{d}} = \widetilde{\mathfrak{d}}_{\mathrm{mid}}$, $\widetilde{\mathfrak{d}} = \widetilde{\mathfrak{d}}^{(LB)}$, and $\widetilde{\mathfrak{d}} = \widetilde{\mathfrak{d}}^{(UB)}$. It can be observed that the vibration amplitudes of the combined structure are significantly reduced compared to the ones of the primary structure for all the considered *PSD* functions. In particular, under the critical seismic excitation, identified by $\widetilde{\mathfrak{d}}^{(c)} = \widetilde{\mathfrak{d}}^{(UB)}$,

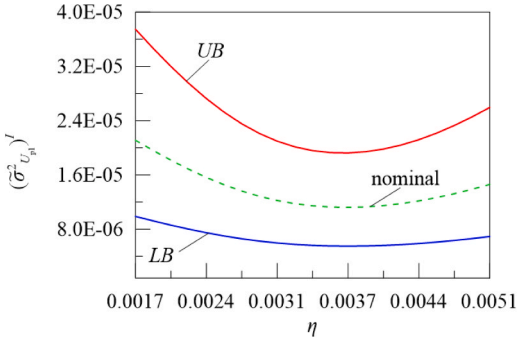

Fig. 8. *LB*, *UB*, and nominal value of the variance of the response process $\widetilde{U}^I_{\mathrm{p1}}(t)$ versus the link stiffness parameter η ($\upsilon = 0.6$).

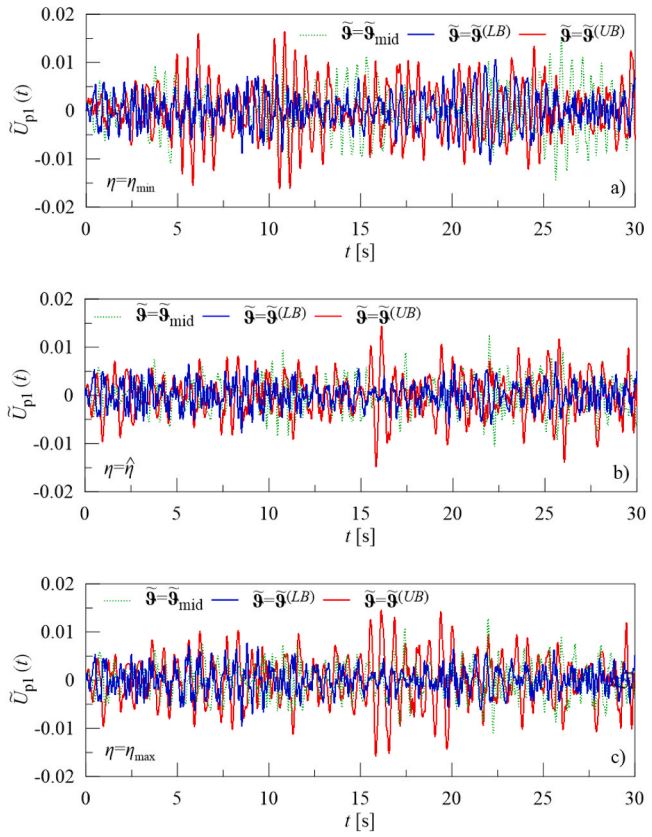

Fig. 9. Samples of the response process $\tilde{U}^I_{\text{p1}}(t)$ of the combined structure for assigned values of the uncertain spectral parameters and different values of the link stiffness ηk_{p}: a) $\eta = \eta_{\min}$; b) $\eta = \hat{\eta}$; and c) $\eta = \eta_{\max}$ ($\upsilon = 0.6$).

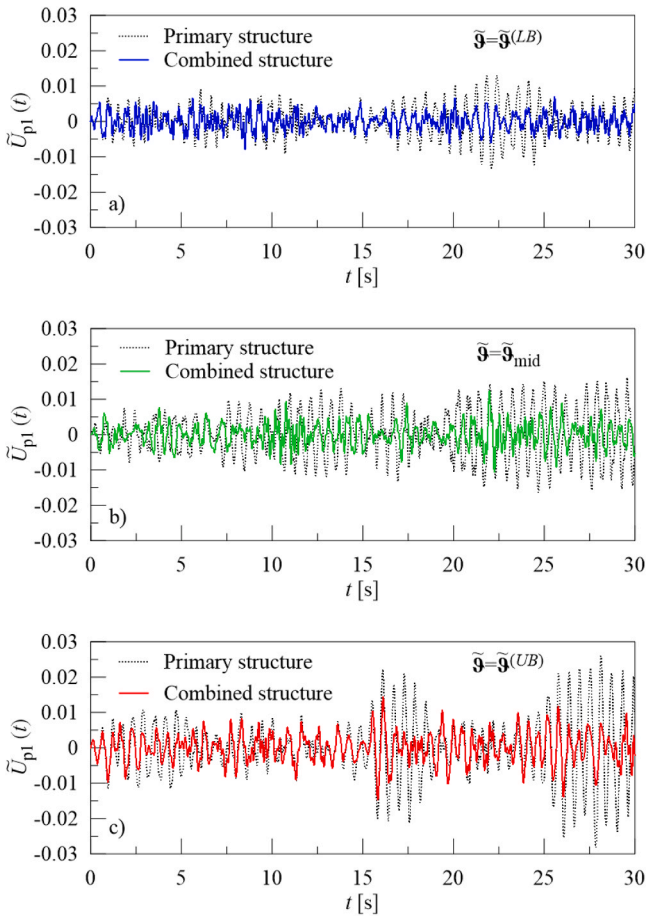

Fig. 10. Samples of the response process $\tilde{U}^I_{\text{p1}}(t)$ of the combined structure contrasted with those of the primary structure for: a) $\tilde{\mathfrak{I}} = \tilde{\mathfrak{I}}^{(LB)}$; b) $\tilde{\mathfrak{I}} = \tilde{\mathfrak{I}}_{\text{mid}}$; and c) $\tilde{\mathfrak{I}} = \tilde{\mathfrak{I}}^{(UB)}$ ($\eta = \hat{\eta}$, $\upsilon = 0.6$).

both the combined and the primary structure exhibit larger vibration amplitudes.

Once the dynamic behavior of the combined structure has been investigated, its seismic performance under imprecise seismic excitation is further assessed by evaluating the bounds of the interval *CDF*, $L^I_{U_{\text{p1,max}}}(b, T)$, and *failure probability*, $P^I_{f,U_{\text{p1,max}}}(b,T)$. The observation time is assumed equal to $T = 30$ s. The accuracy of the bounds given by Eqs. (32a,b) is demonstrated by comparison with the "Exact" ones obtained by a time-consuming combinatorial approach which subdivides the range of the interval parameters into subintervals and screens all possible combinations of the endpoints of the subintervals to seek the minimum and maximum of the *CDF* and *failure probability* for each value of the critical level b. Fig. 11 shows an excellent agreement between the proposed and the "Exact" bounds of the interval *CDF* and *failure probability* for the combined structure with $\eta = \hat{\eta}$ and $\upsilon = 0.6$. The comparison with the nominal solution, pertaining to the midpoint or nominal values of the interval spectral parameters i.e., $\tilde{\mathfrak{I}} = \tilde{\mathfrak{I}}_{\text{mid}}$, shows that neglecting epistemic uncertainties in the seismic excitation may lead to a remarkable overestimation of the safety level compared to the worst-case scenario. Furthermore, it is observed that the region enclosed by the *LB* and *UB* is very wide due to the high degree of uncertainty affecting the three spectral parameters (see Table 2).

To further investigate the influence of the link stiffness ηk_{p} on the vibration capacity control of the secondary subsystems, Fig. 12 displays the *CDF*, $L_{U_{\text{p1,max}}}(b, T)$, and *failure probability*, $P_{f,U_{\text{p1,max}}}(b, T)$, of the combined and primary structure pertaining to the nominal *PSD* function of ground motion acceleration ($\tilde{\mathfrak{I}} = \tilde{\mathfrak{I}}_{\text{mid}}$) for $\eta = \eta_{\min}$, $\eta = \hat{\eta}$, and $\eta = \eta_{\max}$ ($\upsilon = 0.6$). In agreement with the results plotted in Figs. 7–9, it is observed that the best seismic performance is obtained assuming $\eta = \hat{\eta}$ i.e., for the value of the link stiffness parameter which minimizes the variance of the selected response quantity when the other structural parameters are assigned. It is worth mentioning, that the increased safety level of the combined system compared to the primary structure is obtained at the expense of larger displacements of the secondary subsystems. In the context of the design of retrofit solutions based on the use of external subsystems coupled with the main structure, optimal design parameters should be selected so as to limit such displacements.

The influence of imprecision of the seismic excitation on the safety level can be inferred from Fig. 13 where the *LB* and *UB* of the interval *CDF*, $L^I_{U_{\text{p1,max}}}(b, T)$, and *failure probability*, $P^I_{f,U_{\text{p1,max}}}(b, T)$ of the primary structure are compared with the ones of the combined system for three different values of the link stiffness ηk_{p}. Consistently with the previously shown results, the highest safety level is obtained when $\eta = \hat{\eta}$. Notably, for this value of the link stiffness, the region enclosed by the *LB* and *UB* of $L^I_{U_{\text{p1,max}}}(b, T)$ and $P^I_{f,U_{\text{p1,max}}}(b, T)$ is tighter. In general, such a region is wider for the primary structure. Fig. 13 highlights the significant influence of imprecision of the seismic excitation on the performance of both the combined and primary structure. Epistemic uncertainties affecting ground motion acceleration, therefore, should be properly taken into account to assess the vibration control capacity of the secondary subsystems.

6. Conclusions

A novel framework for assessing the performance of combined primary-secondary structures subjected to imprecise seismic excitation has

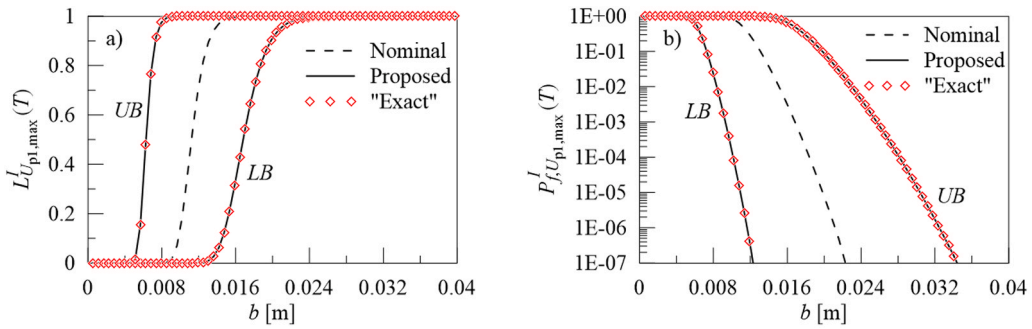

Fig. 11. Bounds of the interval a) *CDF* and b) *failure probability* (in semi-logarithmic scale) of the *extreme value* response process and nominal solution ($\eta = \widehat{\eta}$, $\upsilon = 0.6$).

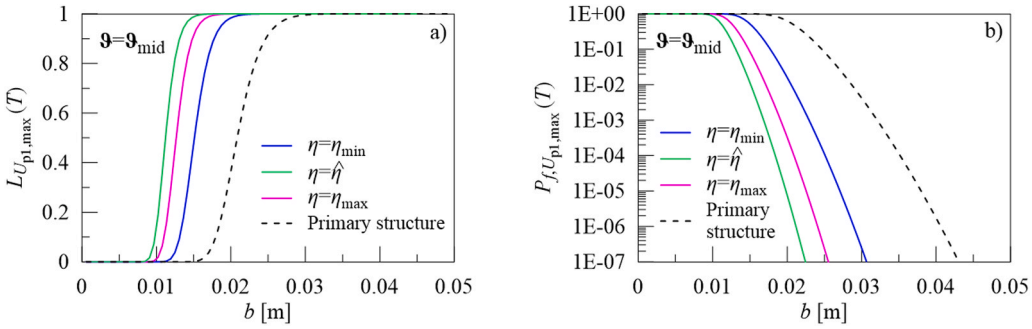

Fig. 12. Nominal a) *CDF* and b) *failure probability* (in semi-logarithmic scale) of the *extreme value* response process $U^I_{p1,max}(T)$ of the combined structure for different values of the link stiffness ηk_p compared with those of the primary structure separately taken ($\upsilon = 0.6$).

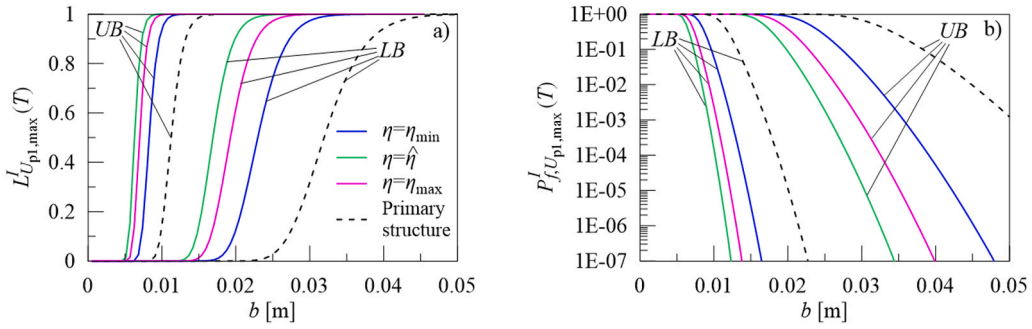

Fig. 13. Proposed bounds of the interval a) *CDF* and b) *failure probability* (in semi-logarithmic scale) of the *extreme value* response process $U^I_{p1,max}(T)$ of the combined structure for different values of the link stiffness ηk_p compared with those of the primary structure separately taken ($\upsilon = 0.6$).

been presented. Ground motion acceleration has been modeled as a zero-mean stationary Gaussian random process, characterized by a recently proposed imprecise *Power Spectral Density* (*PSD*) function depending on three main parameters, which are described as interval variables to account for epistemic uncertainties. The bounds of such variables can be estimated by analyzing a set of recorded accelerograms, which are site-compatible with the area under consideration. Due to the interval nature of the *PSD* function, the dynamic analysis of combined primary-secondary structures under imprecise seismic excitation involves the challenging propagation of hybrid uncertainty i.e., interval and random, which requires the time-consuming solution of a double-loop problem. To address this issue, both frequency- and time-domain formulations of the dynamic problem have been derived. Assuming the variance of the selected response process as a performance indicator, a criterion has been proposed for identifying the seismic excitation leading to the worst-case scenario among all possible realizations of the imprecise ground motion acceleration. In this context, approximate estimates of the bounds of the interval *reliability function* and *failure probability* have been obtained by interval extension of the classical *first-passage* theory.

Numerical results have shown that the vibration amplitude of the primary structure is considerably reduced due to the coupling with the secondary subsystems, which can act as distributed vibration absorbers. The vibration control capacity of the secondary substructures is strongly affected by the stiffness of the links with the primary structure as well as by epistemic uncertainties in the loading model. When secondary subsystems are conceived as seismic retrofit solutions, designers should take into account the imprecision of ground motion acceleration to prevent dangerous overestimation of the vibration control capacity. Since the predominant circular frequency of the imprecise seismic excitation may vary, even for the same soil category, the potential occurrence of resonance conditions with some vibration modes of the combined structural system should be considered at the design stage.

To the best of the authors' knowledge, this study represents the first

effort in the literature devoted to analyzing the influence of the imprecision of seismic excitation on the overall dynamic behavior of combined primary-secondary structures. The proposed framework enables us to efficiently predict the range of structural performance taking into account the inherent random character of ground motion acceleration, epistemic uncertainties affecting the relevant *PSD* function, and the interaction effects between the subsystems.

CRediT authorship contribution statement

Federica Genovese: Writing – review & editing, Visualization, Validation, Software. **Alba Sofi:** Writing – review & editing, Writing – original draft, Visualization, Validation, Supervision, Methodology, Conceptualization.

Declaration of Competing Interest

The authors declare that they have no known competing financial interests or personal relationships that could have appeared to influence the work reported in this paper.

Data availability

Data will be made available on request.

Acknowledgment

The support to this research by the European Union—FSE-REACT-EU, PON Research and Innovation 2014–2020 DM1062/2021 is gratefully acknowledged.

Appendix A. Parameters of the *Power Spectral Density* function of ground motion acceleration

The interval parameter β_0^I is defined by interval extension of the expression given in Ref. [42]:

$$\beta_0 = \frac{2a_0\, b_0 \left(\omega_H^4 + \omega_L^4\right)}{\omega_L^3 (c_0 + d_0 + e_0)} \tag{A.1}$$

where:

$$\begin{aligned}
a_0 &= \left(\rho_0^2 + \Omega_0^2\right)^4 + 2\left(\rho_0^4 - 6\,\rho_0^2\,\Omega_0^2 + \Omega_0^4\right)\omega_L^4 + \omega_L^8;\\
b_0 &= \rho_0^4 + 2\,\rho_0^2\left(\Omega_0^2 - \omega_H^2\right) + \left(\Omega_0^2 + \omega_H^2\right)^2;\\
c_0 &= -2\,a_0\,\rho_0\,\omega_H\,\omega_L\left(\rho_0^2 + \Omega_0^2 - \omega_H^2\right);\\
d_0 &= \left\{\left(\rho_0^2 + \Omega_0^2\right)^2\left(\rho_0^4 - 6\,\rho_0^2\,\Omega_0^2 + \Omega_0^4 + \omega_L^4\right) - \omega_H^2\left(\rho_0^2 - \Omega_0^2\right)\left[\left(\rho_0^2 + \Omega_0^2\right)^2 + \omega_L^4\right]\right\} \times 2\omega_L\left(\omega_H^4 + \omega_L^4\right);\\
e_0 &= \sqrt{2} b_0\,\rho_0\left\{\omega_L^2\left(\omega_H^2 - \omega_L^2\right)\left(\omega_L^4 + \rho_0^4 - 2\,\rho_0^2\,\Omega_0^2 - 3\,\Omega_0^4\right) + \left(\omega_H^2 + \omega_L^2\right)\left[\rho_0^6 + \Omega_0^6 + 3\,\Omega_0^2\,\rho_0^2\left(\rho_0^2 + \Omega_0^2\right) + \omega_L^4\left(\rho_0^2 - 3\,\Omega_0^2\right)\right]\right\}
\end{aligned} \tag{A.2a-e}$$

where ω_H and ω_L can be assumed equal to $\omega_H = 0.1\,\Omega_0$ and $\omega_L = \Omega_0 + 0.8\rho_0$, respectively.

Appendix B. Step-by-step integration of the equations of motion

The response sample of the combined primary-secondary structure subjected to the $k-$th sample of the seismic acceleration $\ddot{U}_g^{(k)}\left(t;\boldsymbol{\vartheta}^{(j)}\right)$ generated from the $j-$th realization of the interval *PSD* function $G_{\ddot{U}_g}\left(\omega;\boldsymbol{\vartheta}^{(j)}\right)$ (Eq. (27)) can be obtained by solving Eq. (26) through a step-by-step scheme. Subdividing the time interval of interest $[0, T_f]$ into N_t small intervals of equal amplitude $\Delta t = T_f/N_t$ and assuming that seismic acceleration is piecewise linear within each time interval, the modal state variable vector at the time instant $t_{\ell+1} = (\ell+1)\Delta t$ can be evaluated as [52]:

$$\mathbf{X}^{(k)}\left(t_{\ell+1};\boldsymbol{\vartheta}^{(j)}\right) = \exp(\boldsymbol{\Lambda}\,\Delta t)\mathbf{X}^{(k)}\left(t_\ell;\boldsymbol{\vartheta}^{(j)}\right) + \boldsymbol{\gamma}_0(\Delta t)\mathbf{v}\,\ddot{U}_g\left(t_\ell;\boldsymbol{\vartheta}^{(j)}\right) + \boldsymbol{\gamma}_1(\Delta t)\mathbf{v}\,\ddot{U}_g\left(t_{\ell+1};\boldsymbol{\vartheta}^{(j)}\right) \tag{B.1}$$

where

$$\boldsymbol{\gamma}_0(\Delta t) = \left[\exp(\boldsymbol{\Lambda}\,\Delta t) - \frac{\mathbf{L}(\Delta t)}{\Delta t}\right]\boldsymbol{\Lambda}^{-1} \tag{B.2}$$

$$\boldsymbol{\gamma}_1(\Delta t) = \left[\frac{\mathbf{L}(\Delta t)}{\Delta t} - \mathbf{I}_{2m}\right]\boldsymbol{\Lambda}^{-1} \tag{B.3}$$

with

$$\mathbf{L}(\Delta t) = [\exp(\boldsymbol{\Lambda}\,\Delta t) - \mathbf{I}_{2m}]\boldsymbol{\Lambda}^{-1} \tag{B.4}$$

$\mathbf{I}_{2m}$ being the $2m-$order identity matrix.

Then, based on the knowledge of $\mathbf{X}^{(k)}(t_{\ell+1};\boldsymbol{\vartheta}^{(j)})$, the state variable vector in the nodal space at the time instant $t_{\ell+1}$ can be derived by applying Eq. (25), i.e.:

$$\mathbf{Z}^{(k)}\left(t_{\ell+1};\boldsymbol{\vartheta}^{(j)}\right) = \boldsymbol{\Upsilon}\,\mathbf{X}^{(k)}\left(t_{\ell+1};\boldsymbol{\vartheta}^{(j)}\right). \tag{B.5}$$

References

[1] Shinozuka M, Deodatis G. Simulation of stochastic processes by spectral representation. Appl Mech Rev 1991;44(4):191–204. https://doi.org/10.1115/1.3119501.

[2] Liang J, Chaudhuri SR, Shinozuka M. Simulation of nonstationary stochastic processes by spectral representation. J Eng Mech 2007;133(6):616–27. https://doi.org/10.1061/(ASCE)0733-9399(2007)133:6(616).

[3] Zio E. The Monte Carlo Simulation Method for System Reliability and Risk Analysis. Springer London,; 2013. https://doi.org/10.1007/978-1-4471-4588-2.

[4] Schuëller GI. Efficient Monte Carlo simulation procedures in structural uncertainty and reliability analysis - recent advances. Struct Eng Mech 2009;32(1):1–20. https://doi.org/10.12989/sem.2009.32.1.001.

[5] Song C, Kawai R. Monte Carlo and variance reduction methods for structural reliability analysis: a comprehensive review. Probab Eng Mech 2023;73:103479. https://doi.org/10.1016/j.probengmech.2023.103479.

[6] Vanmarcke EH, Lai SSP. Strong-motion duration and RMS amplitude of earthquake records. Bull Seismol Soc Am 1980;70(4):1293–307.

[7] Luco JE. Lower bounds for peak horizontal strong-motion amplitudes. Bull Seism Soc Am 1980;70(4):1309–20.

[8] Lai SSP. Statistical characterization of strong ground motions using power spectral density function. Bull Seism Soc Am 1982;72(1):259–74.

[9] Comerford L, Kougioumtzoglou IA, Beer M. An artificial neural network approach for stochastic process power spectrum estimation subject to missing data. Struct Saf 2015;52:150–60. https://doi.org/10.1016/j.strusafe.2014.10.001.

[10] Comerford L, Kougioumtzoglou IA, Beer M. Compressive sensing based stochastic process power spectrum estimation subject to missing data. Probab Eng Mech 2016;44:66–76. https://doi.org/10.1016/j.probengmech.2015.09.015.

[11] Zhang Y, Comerford L, Kougioumtzoglou IA, Patelli E. Uncertainty quantification of power spectrum and spectral moments estimates subject to missing data. ASCE-ASME J Risk Uncertain Eng Syst, Part A: Civ Eng 2017;3(4):04017020. https://doi.org/10.1061/AJRUA6.0000925.

[12] Muscolino G, Genovese F, Sofi A. Reliability bounds for structural systems subjected to a set of recorded accelerograms leading to imprecise seismic power spectrum. ASCE-ASME J Risk Uncertain Eng Syst, Part A: Civ Eng 2022;8(2):04022009. https://doi.org/10.1061/AJRUA6.0001215.

[13] Behrendt M, Dang C, Beer M. Data-driven and physics-based interval modelling of power spectral density functions from limited data. Mech Syst Signal Process 2024;208:111078. https://doi.org/10.1016/j.ymssp.2023.111078.

[14] Behrendt M, Bittner M, Comerford L, Beer M, Chen J. Relaxed power spectrum estimation from multiple data records utilising subjective probabilities. Mech Syst Signal Process 2022;165:108346. https://doi.org/10.1016/j.ymssp.2021.108346.

[15] Bittner M, Behrendt M, Beer M. Relaxed evolutionary power spectral density functions: a probabilistic approach to model uncertainties of non-stationary stochastic signals. Mech Syst Signal Process 2024;211:111210. https://doi.org/10.1016/j.ymssp.2024.111210.

[16] Behrendt M, Faes MGR, Valdebenito MA, Beer M. Estimation of an imprecise power spectral density function with optimised bounds from scarce data for epistemic uncertainty quantification. Mech Syst Signal Process 2023;189:110072. https://doi.org/10.1016/j.ymssp.2022.110072.

[17] Muscolino G. Dynamic response of multiply connected primary-secondary systems. Earthq Eng Struct Dyn 1990;19(2):205–16. https://doi.org/10.1002/eqe.4290190205.

[18] Biondi B, Muscolino G. Component-mode synthesis method variants in the dynamics of coupled structures. Meccanica 2000;35(1):17–38. https://doi.org/10.1023/A:1004730011796.

[19] Yaohua Z, Qizhi L. A study on the interaction between the primary and secondary structures of combined structures. J Sound Vib 2000;234(3):529–45. https://doi.org/10.1006/jsvi.2000.2952.

[20] Biondi B, Muscolino G. Component-mode synthesis method for coupled continuous and FE discretized substructures. Eng Struct 2003;25:419–33. https://doi.org/10.1016/S0141-0296(02)00183-9.

[21] Den Hartog JP. Mechanical Vibrations. New York: Mc-Graw Hill,; 1956.

[22] Moon KS. Tall building motion control using double skin façades. J Arch Eng 2009;15(3):84–90. https://doi.org/10.1061/(ASCE)1076-0431(2009)15:3(84).

[23] Moon KS. Structural design of double skin facades as damping devices for tall buildings. Procedia Eng 2011;14:1351–8. https://doi.org/10.1016/j.proeng.2011.07.170.

[24] Fu TS, Zhang R. Integrating double-skin façades and mass dampers for structural safety and energy efficiency. J Arch Eng 2016;22:1–12. https://doi.org/10.1061/(ASCE)AE.1943-5568.0000218.

[25] Bedon C, Amadio C. Enhancement of the seismic performance of multi-storey buildings by means of dissipative glazing curtain walls. Eng Struct 2017;152(1):320–34. https://doi.org/10.1016/j.engstruct.2017.09.028.

[26] Bedon C, Amadio C. Numerical assessment of vibration control systems for multihazard design and mitigation of glass curtain walls. J Build Eng 2018;15:1–13. https://doi.org/10.1016/j.jobe.2017.11.004.

[27] Pipitone G, Barone G, Palmeri A. Optimal design of double-skin façades as vibration absorbers. Struct Contr Health Monit 2018;25(2):e2086. https://doi.org/10.1002/stc.2086.

[28] Pipitone G, Barone G, Palmeri A. Stochastic design of double-skin façades as seismic vibration absorbers. Adv Eng Softw 2020;142:102749. https://doi.org/10.1016/j.advengsoft.2019.102749.

[29] Di Giovanni G, Bernardini D. Vibration damping performances of buildings with moving façades under harmonic excitation. J Vib Eng Technol 2023;11:381–90. https://doi.org/10.1007/s42417-020-00247-w.

[30] Fina M, Lauff C, Faes MGR, Valdebenito MA, Wagner W, Freitag S. Bounding imprecise failure probabilities in structural mechanics based on maximum standard deviation. Struct Saf 2023;101:102293. https://doi.org/10.1016/j.strusafe.2022.102293.

[31] Moore RE, Kearfott RB, Cloud MJ. Introduction to interval analysis. Philos: SIAM 2009.

[32] De Angelis M, Patelli E, Beer M. Advanced line sampling for efficient robust reliability analysis. Struct Saf 2015;52:170–82. https://doi.org/10.1016/j.strusafe.2014.10.002.

[33] Wei P, Lu Z, Song J. Extended Monte Carlo simulation for parametric global sensitivity analysis and optimization. AIAA J 2014;52(4):867–78. https://doi.org/10.2514/1.J052726.

[34] Wei P, Song J, Bi S, Broggi M, Beer M, Lu Z, et al. Non-intrusive stochastic analysis with parameterized imprecise probability models: I. Performance estimation. Mech Syst Signal Process 2019;124:349–68. https://doi.org/10.1016/j.ymssp.2019.01.058.

[35] Wei P, Liu F, Valdebenito M, Beer M. Bayesian probabilistic propagation of imprecise probabilities with large epistemic uncertainty. Mech Syst Signal Process 2021;149:107219. https://doi.org/10.1016/j.ymssp.2020.107219.

[36] Faes MGR, Valdebenito MA, Moens D, Beer M. Bounding the first excursion probability of linear structures subjected to imprecise stochastic loading. Comput Struct 2020;239:106320. https://doi.org/10.1016/j.compstruc.2020.106320.

[37] Faes MGR, Valdebenito MA, Moens D, Beer M. Operator norm theory as an efficient tool to propagate hybrid uncertainties and calculate imprecise probabilities. Mech Syst Signal Process 2021;1521:107482. https://doi.org/10.1016/j.ymssp.2020.107482.

[38] Jiang C, Zheng J, Han X. Probability-interval hybrid uncertainty analysis for structures with both aleatory and epistemic uncertainties: a review. Struct Multidiscip Optim 2018;57(6):2485–502. https://doi.org/10.1007/s00158-017-1864-4.

[39] Faes M, Daub M, Marelli S, Patelli E, Beer M. Engineering analysis with probability boxes: a review on computational methods. Struct Saf 2021;93:102092. https://doi.org/10.1016/j.strusafe.2021.102092.

[40] Lutes LD, Sarkani S. Stochastic Analysis of Structural and Mechanical Vibrations. N.J.: Prentice-Hall, Upper Saddle River,; 1997.

[41] Li J, Chen JB. Stochastic Dynamics of Structures. Singapore: John Wiley & Sons,; 2009.

[42] Muscolino G, Genovese F, Biondi G, Cascone E. Generation of fully non-stationary random processes consistent with target seismic accelerograms. Soil Dyn Earthq Eng 2021;141:106467. https://doi.org/10.1016/j.soildyn.2020.106467.

[43] Conte JP, Peng BF. Fully nonstationary analytical earthquake ground-motion model. J Eng Mech 1997;123(1):15–24. https://doi.org/10.1061/(ASCE)0733-9399.

[44] Muscolino G, Sofi A. Stochastic response of structures with uncertain-but-bounded parameters via improved interval analysis. Probab Eng Mech 2012;28:152–63. https://doi.org/10.1016/j.probengmech.2011.08.011.

[45] Borino G, Muscolino G. Mode-superposition methods in dynamic analysis of classically damped linear systems. Earthq Eng Struct Dyn 1986;14(5):705–17. https://doi.org/10.1002/eqe.4290140503.

[46] Muscolino G. Dynamically modified linear structures: deterministic and stochastic response. J Eng Mech Div (ASCE 1996;122(11):1044–51. https://doi.org/10.1061/(ASCE)0733-9399(1996)122:11(1044).

[47] Vanmarcke EH. On the distribution of the first-passage time for normal stationary random processes. J Appl Mech 1975;42(1):215–20. https://doi.org/10.1115/1.3423521.

[48] Stucchi M, Meletti C, Montaldo V, Crowley H, Calvi GM, Boschi E. Seismic hazard assessment (2003-2009) for the Italian building code. Bull Seismol Soc Am 2011;101(4):1885–911. https://doi.org/10.1785/0120100130.

[49] Weatherill G, Burton PW. An alternative approach to probabilistic seismic hazard analysis in the Aegean region using Monte Carlo simulation. Tectonophysics 2010;492(1–4):253–78. https://doi.org/10.1016/j.tecto.2010.06.022.

[50] Ancheta TD, Darragh RB, Stewart JP, Seyhan E, Silva WJ, Chiou BSJ, et al. NGA-West2 database. Earthq Spectra 2014;30(3):989–1005. https://doi.org/10.1193/070913EQS197M.

[51] Luzi L. , Lanzano G. , Felicetta C. , D'Amico M.C. , Russo E. , Sgobba S., et al. 5. Engineering strong motion database (ESM) (version 2.0). Rome: National Institute of Geophysics and Volcanology; 2020. https://doi.org/10.13127/ESM.2.

[52] D'Aveni A, Muscolino G. Improved dynamic correction method in seismic analysis of both classically and non-classically damped structures. Earthq Eng Struct Dyn 2001;30(4):501–17. https://doi.org/10.1002/eqe.20.